machines

MDPI

Article

Research on Capacity Parameter Matching and Robust Design of a Methanol Range-Extended Series Hybrid Powertrain System for Harbor Tugs

Zhao Li, Hua Tian and Wuqiang Long *

School of Energy and Power Engineering, Dalian University of Technology, Dalian 116081, China; lizhao@mail.dlut.edu.cn (Z.L.); tianhua@dlut.edu.cn (H.T.)
* Correspondence: longwq@dlut.edu.cn; Tel.: +86-13889538768

Abstract

To address the stringent emission regulations of the International Maritime Organization (IMO) and the growing demand for green port operations, this study proposes an innovative range-extended series hybrid powertrain system featuring a dedicated methanol engine as an Auxiliary Power Unit (APU) for harbor tugs. Based on an analysis of actual ship operational data, a core design paradigm of "battery-dominant, engine-as-range-extender" is established. A robust capacity parameter matching method is proposed, yielding a configuration comprising a 200 kW·h/600 kW Lithium Iron Phosphate Battery Pack (LFPBP), a 250 kW methanol APU, and a 400/600 kW Permanent Magnet Synchronous Propulsion Motor (PMSM). A hierarchical intelligent energy management strategy (EMS), integrating state-machine coordination and real-time power allocation, is designed. High-fidelity simulations under a typical duty cycle demonstrate that the proposed system achieves an equivalent fuel-saving rate of 50.8% compared with a conventional diesel system, with the engine operating exclusively in its high-efficiency zone (>42% efficiency) for only 35% of the operational time. A full life-cycle techno-economic analysis reveals an incremental investment payback period (PBP) of approximately 3 months and a net present value (NPV) exceeding USD 9.69 million over a 10-year period. Quantitative environmental analysis shows an annual reduction of approximately 94.8% in CO_2 emissions (assuming the use of green methanol produced from renewable sources and captured CO_2), 95% in NO_x emissions, and the near-elimination of SO_x and particulate matter (PM). This study provides a systematic and economically attractive solution with promising engineering feasibility verified by simulation, which paves the way for further experimental validation and practical engineering implementation.

Keywords: harbor tug; methanol; range-extended series hybrid powertrain; parameter matching; robust design; energy management strategy

Check for updates

Academic Editor: Ahmed Abu-Siada

Received: 3 February 2026
Revised: 26 February 2026
Accepted: 28 February 2026
Published: 2 March 2026

Copyright: © 2026 by the authors. Licensee MDPI, Basel, Switzerland. This article is an open access article distributed under the terms and conditions of the Creative Commons Attribution (CC BY) license.

1. Introduction

Ports, as critical nodes of global trade and logistics, are placing increasing emphasis on their environmental performance and operational sustainability [1]. Harbor tugs, which assist large ships in safe berthing/unberthing and intra-port operations, have powertrain systems whose efficiency directly determines the reliability, economic efficiency, and environmental friendliness of port operations [2]. However, the operational profile of such vessels is highly challenging, characterized by frequent starts, accelerations, decelerations,

turns, and short-term high-load towing, which results in traditional powertrains operating under inefficient conditions for prolonged periods [3]. The widely used medium/high-speed diesel direct mechanical propulsion systems operate far from their designed efficient points for long durations under such highly variable and low-average-load conditions, leading to a significant increase in fuel consumption rates [4]. Concurrently, incomplete combustion generates substantial nitrogen oxides (NO_x), sulfur oxides (SO_x), particulate matter (PM), and carbon dioxide (CO_2) emissions, making harbor tugs a major mobile pollution source for ports and adjacent coastal areas [5].

Faced with the increasingly stringent emission regulations of the IMO (e.g., MARPOL Annex VI Tier III standards) and the urgent pressure of the global shipping industry's "carbon neutrality" strategy, the development of green and efficient new marine powertrain systems has become an industry consensus and an inevitable choice [6,7]. For instance, IMO Tier III standards mandate a significant reduction in NO_x emissions for ships operating in Emission Control Areas (ECAs) [8]. While traditional diesel engines can meet these standards with expensive aftertreatment systems such as Selective Catalytic Reduction (SCR), alternative fuels and hybrid powertrain concepts offer pathways for cleaner combustion at the source [9,10]. It is within this regulatory and technological landscape that the methanol hybrid system proposed in this study finds its practical relevance.

Literature Review

The pursuit of green and efficient marine propulsion is driven by increasingly stringent international regulations, including the IMO Tier III standards for NO_x control and the broader decarbonization targets of the shipping industry. Within this regulatory landscape, a variety of technological pathways have been explored, among which hybrid power technology (particularly the range-extended series configuration) has emerged as a promising solution due to its ability to decouple the prime mover from transient load demands [11]. In this configuration, the prime mover (engine) and the propulsor (propeller) are mechanically decoupled; the engine solely drives a generator to produce electricity, and this electrical energy, combined with the output from the energy storage device, drives the propulsion motor via power electronics [12]. This "electric drive" architecture completely liberates the engine from the complex dynamic loads of the propeller, enabling it to operate continuously and stably at a preset high-efficiency, low-emission operating point, thus significantly improving the overall energy efficiency and emission performance across all operational conditions [13]. Simultaneously, high-power-density lithium-ion battery packs act as the system's "power buffer" and primary energy source, responding instantaneously to severe load fluctuations, providing excellent acceleration performance, and efficiently recovering ship braking energy to form an energy-saving loop [14]. The degree of hybridization and the choice of powertrain topology (series, parallel, or series–parallel) significantly impact overall efficiency [15–18], as demonstrated by Milićević et al. [19] in their numerical analysis of hybrid electric powertrains, which highlights the importance of optimal component sizing for specific operational cycles.

Parallel to powertrain hybridization, fuel selection is equally critical. Methanol has emerged as a leading candidate among alternative marine fuels due to its ambient liquid state, ease of storage and bunkering, and potential for carbon-neutral production via e-methanol pathways [20–22]. Its combustion produces negligible SO_x and PM, and significantly lower NO_x compared with conventional heavy fuel oil [23]. When integrated into a hybrid architecture, the clean combustion characteristics of methanol can be further amplified by enabling the engine to operate exclusively at steady-state, high-efficiency points, thereby minimizing transient emissions [24]. This synergy between fuel choice and powertrain topology is particularly relevant for vessels such as harbor tugs, which face

highly variable load profiles. To substantiate this potential, a quantitative understanding of the unique operational profile of harbor tugs is essential. By integrating actual ship voyage data with hydrodynamic principles, this study first establishes a variable-load power demand model. The analysis reveals distinct characteristics of harbor tug operations: a large peak-to-valley power difference (peak power 633.2 kW vs. average power 189.9 kW), severe and frequent load fluctuations (standard deviation 128.4 kW), and a consistently low average load factor (30.0%), with approximately 86.8% of operating time spent below 300 kW. These quantitative findings underscore the inherent inefficiency of conventional diesel direct-drive systems and provide the foundational basis for the design of a hybrid solution.

Despite the promising prospects, the successful application of methanol range-extended series hybrid systems on harbor tugs still faces a series of key scientific and engineering challenges, with the core lying in the lack of a scientific, systematic, and robust methodology for capacity parameter matching and integrated design. The rationality of parameter matching is the cornerstone determining system performance, economic viability, and reliability [25]. Battery capacity and power require an optimal trade-off between pure electric range, power buffer requirements, cost, and space constraints [26]; the power of the methanol engine–generator set (APU) needs to balance efficient power generation capability with system redundancy [27]; and the performance of the EMS directly determines whether the theoretical parametric advantages can be translated into actual operational benefits [28]. Although existing research has explored parameter optimization and energy management for vehicle hybrid systems—for example, Wang et al. proposed a hierarchical optimization method for plug-in hybrid electric buses (PHEBs), significantly improving fuel economy and battery protection through the co-optimization of EMS and powertrain parameters [29]. Bai et al. proposed a multi-dimensional sizing optimization framework and hierarchical EMS (HEMS) for plug-in hybrid electric vehicles (PHEVs) with hybrid energy storage systems (HESS), improving both vehicle economic efficiency and battery life by optimizing component sizes and power allocation [30]. Zhu et al. proposed a multi-objective bi-level optimization method for the simultaneous co-optimization of component sizing and energy management for hybrid electric propulsion systems [31]. In-depth research specifically targeting methanol range-extended series hybrid systems for harbor tugs with distinct "variable-load, large peak-valley difference, low average load" operational characteristics remains relatively scarce. This is especially true for key component parameter matching based on accurate load characteristic analysis, robust optimization design considering uncertainties, and comprehensive life-cycle assessment. Existing studies have not yet formed a systematic, publicly available design methodology or detailed case references. How to establish quantitative design criteria for the synergistic matching of component capacities and further design an EMS that balances real-time performance, robustness, and global optimality remains a gap in current research. While previous research has advanced hybrid electric vehicle (HEV) design, a systematic methodology for methanol range-extended series hybrid systems in harbor tugs remains underdeveloped, including integrated parameter optimization under real-world operating conditions, layered energy management, and a complete life-cycle techno-economic evaluation.

To address the aforementioned research gaps, this study aims to construct a complete design methodology and solution for methanol range-extended series hybrid systems for harbor tugs, encompassing core modeling, robust parameter matching, intelligent energy management, and full life-cycle assessment. Specifically, this study first establishes a high-precision variable-load power demand prediction model based on actual ship operation data and hydrodynamic principles to accurately quantify load statistical characteristics. Based on this model, a robust power component capacity parameter matching method

targeting global optimal energy efficiency, minimum life-cycle cost, and maximum system robustness is proposed. Subsequently, a hierarchical intelligent EMS capable of balancing real-time response and global optimization is designed. The effectiveness of the research scheme is validated through high-fidelity system simulation, with a focus on evaluating dynamic performance, energy-saving, and emission reduction effects under typical duty cycles. Simultaneously, comprehensive techno-economic and environmental benefit assessment models are constructed to quantify the commercial value and emission reduction contribution of the proposed scheme. Ultimately, this study aims to provide ship designers, port operators, and policymakers with a reference framework from theoretical methods to engineering practice, actively promoting the green and intelligent transformation of port operation vessels.

The main scientific contributions and innovations of this study, which directly address the identified research gaps and distinguish it from existing hybrid tug designs, are summarized as follows:

1. A systematic, data-driven design methodology for range-extended hybrid powertrains tailored to the unique operational profile of harbor tugs. This methodology integrates multi-source data fusion for high-fidelity load profiling with a robust, multi-constraint parameter matching process, moving beyond empirical selection to a demand-driven approach.
2. A novel "battery-dominant, engine-as-efficient-APU" design paradigm that quantitatively justifies the decoupling of energy and power. By allocating transient load buffering to the battery and steady-state power generation to the methanol engine, the system intrinsically resolves the conflict between the engine's need for stable operation and the propeller's highly fluctuating load demand.
3. A hierarchical and intelligent EMS that combines the robustness of rule-based mode coordination with the optimization capability of real-time power allocation. This EMS is specifically designed to leverage the hardware architecture, ensuring the practical realization of the theoretical efficiency gains.
4. A comprehensive validation and assessment framework that goes beyond single-metric evaluation. It holistically assesses the proposed system through high-fidelity dynamic simulation, full life-cycle techno-economic analysis (including sensitivity analysis), and detailed environmental impact quantification, thereby providing a multi-faceted proof of concept.

2. System Configuration, Modeling, and Design Methodology

2.1. Overall System Configuration and Core Design Principles

The overall configuration of the methanol range-extended series hybrid powertrain system proposed in this study is shown in Figure 1. The system adopts a centralized power distribution architecture based on a 1000 V Direct Current (DC) bus, integrating power generation, energy storage, propulsion, and auxiliary loads. Within this architecture, the methanol engine is strictly designated as part of the APU and is mechanically decoupled from the propeller; its sole function is to drive the generator to produce electrical power, thereby serving as a range extender rather than a prime mover for direct propulsion. This architecture offers advantages such as a clear structure, flexible control, and ease of redundancy expansion.

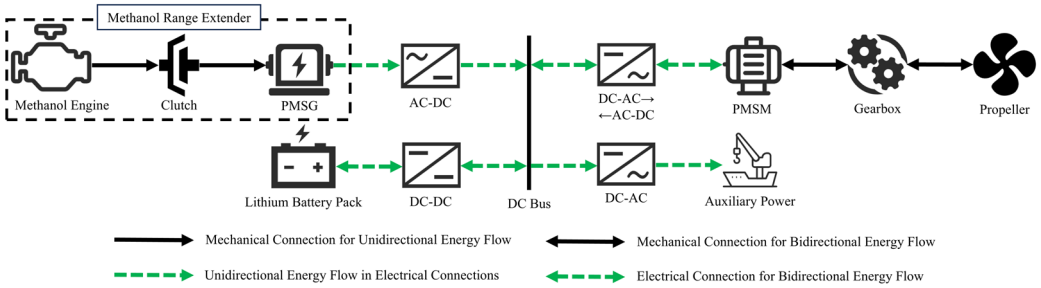

Figure 1. Topology of the methanol range-extended series hybrid powertrain system.

The design and operation of the system adhere to the following four core principles, aiming to systematically address the inherent defects of traditional powertrain systems.

(a) "Battery Priority, Clean Operation" Principle: When the battery State of Charge (SOC) is within a safe and efficient window, all power demands of the vessel (including propulsion and onboard auxiliary systems) are independently supplied by the Lithium Iron Phosphate Battery Pack (LFPBP). This ensures the tug can operate with local zero emissions and low noise for most operations in core port areas and sensitive ecological zones, maximizing environmental benefits.

(b) "Engine as Efficient, Steady-State APU" Principle: The methanol engine is rigidly coupled with the generator to form the APU, whose function is strictly defined as an "on-demand charging source". It starts only when battery energy is insufficient, or the load demand exceeds the battery's instantaneous supply capability. Once started, it is controlled to operate near its rated power point (e.g., 90–100% of rated power) in the high-efficiency flat region, outputting electrical power at a constant rate and completely avoiding inefficient, high-emission transient and low-load operating conditions.

(c) "Battery as Dynamic Power Filter and Energy Pool" Principle: The lithium battery pack serves a dual role. First, as a "power filter", it utilizes its millisecond-level power response capability to instantaneously absorb or release power, smoothing the severe fluctuations of the propeller load, thereby creating an ideal, steady-state power generation environment for the engine. Second, as an "energy pool", it stores surplus generated energy and regenerated braking energy, releasing it during high-power demand periods, thus extending the engine's high-efficiency operating time window.

(d) "Intelligent Coordination, Global Optimization" Principle: By deploying an advanced energy management system, based on real-time monitoring of system states (SOC, power demand, component temperatures, etc.) and preset optimization objectives (e.g., minimum equivalent fuel consumption, minimum emissions, battery life protection), intelligent decisions are made regarding engine start/stop timing, real-time power allocation among energy sources, utilization of regenerated braking energy, etc., ensuring the system always operates in an optimal or near-optimal state in terms of safety, efficiency, and economic viability.

2.2. Refined Power Demand Modeling and Analysis Based on Multi-Source Data

Accurate ship power demand profiling is a prerequisite for scientific parameter matching. This study comprehensively utilizes parent ship data, actual ship voyage data records (Automatic Identification System, AIS/Voyage Data Recorder, VDR data segments), and ship principal-based calculations to construct a complete analysis chain from operational tasks to electrical power demand at the DC bus side.

2.2.1. Ship Resistance and Propulsion Power Calculation Model

A simplified modified formula based on the Holtrop–Mennen method is used to estimate the total resistance R_t:

$$R_t = R_f(1 + k_1) + R_{app} + R_w, \quad (1)$$

where R_f is frictional resistance, calculated according to the ITTC-1957 formula; k_1 is the form factor; R_{app} is appendage resistance; R_w is the wave-making resistance. For harbor tugs, the Froude number is typically below 0.3, making wave-making resistance relatively small; resistance is dominated by frictional and residual components. The model was calibrated against the known power–speed relationship of the parent tug at its design speed (e.g., 12 knots), ensuring that the predicted resistance matches the actual delivered power at that point. Based on the principal dimensions (length ~35 m, beam ~10 m, draft ~4 m) and reference data for similar tug hull forms from published systematic series (e.g., [32]), the total resistance coefficient C_t in the typical operating speed range is estimated as 3.5×10^{-3}. This value is consistent with coefficients reported for comparable tugboats in the literature.

The relationship between the delivered power to the propeller P_D and effective power P_E is:

$$P_D = \frac{P_E}{\eta_0 \cdot \eta_R \cdot \eta_H} = \frac{R_t \cdot V}{\eta_0 \cdot \eta_R \cdot \eta_H}, \quad (2)$$

where V is the speed (m/s); η_0 is the propeller open water efficiency, approximately 0.65 at the design point for the selected Modified Au-type (MAU) propeller based on diagrams; η_R is the relative rotative efficiency, taken as 0.98; η_H is the hull efficiency, taken as 1.05 considering the tug's hull form characteristics (indicating the wake fraction exceeds the thrust deduction fraction). A hull efficiency greater than 1 is not uncommon for tugboats, which often feature full hull forms and large, heavily loaded propellers operating in a high wake fraction environment. In such cases, the wake fraction (w) can significantly exceed the thrust deduction fraction (t), leading to an efficiency gain from the hull–propeller interaction ($\eta_H = (1 - t)/(1 - w) > 1$). This relationship between effective power and delivered power follows standard naval architecture principles, with the efficiency components derived from propeller open-water tests and hull–propeller interaction coefficients [32].

2.2.2. Electric Propulsion Chain Efficiency Modeling

Power transmission from the DC bus to the propeller involves multiple conversion stages. The total efficiency $\eta_{prop,elec}$ is the product of individual stage efficiencies:

$$\eta_{prop,elec} = \eta_{inv} \cdot \eta_{motor} \cdot \eta_{gb} \cdot \eta_{shaft}, \quad (3)$$

where η_{inv} is propulsion inverter efficiency, with a typical value of 0.98; η_{motor} is the Permanent Magnet Synchronous Motor (PMSM) efficiency, maintainable between 0.95 and 0.97 over a wide load range, with an average value taken as 0.96; η_{gb} is the gearbox efficiency, taken as 0.97; η_{shaft} is the shafting efficiency, taken as 0.98. Therefore, $\eta_{prop,elec} \approx 0.89$. The efficiencies for each component in the electric propulsion chain are typical values for modern marine power systems, as documented in the literature on all-electric ships [33].

2.2.3. Auxiliary System Power and Total Electrical Power Demand

Ship auxiliary system power P_{aux} includes the steering gear, thruster, hydraulic system, control system, lighting, ventilation/air conditioning, etc. Based on the equipment list estimation, under typical operational conditions, P_{aux} fluctuates approximately within the 40–60 kW range. This study uses the average value $\overline{P_{aux}} = 50$ kW for preliminary design [34].

Therefore, the total electrical power $P_{DC,req}$ that needs to be provided by the DC bus is:

$$P_{DC,\ req} = \frac{P_D}{\eta_{prop,elec}} + P_{aux}, \tag{4}$$

2.2.4. Typical Duty Cycle Power Demand Characteristic Analysis

This study constructs a representative 3600 s (1 h) duty cycle for a harbor tug. This cycle is synthesized by concatenating typical operational segments derived from the analysis of long-term AIS and VDR data from the parent vessel, and is designed to be a realistic and compact representation of the tug's daily activities, including the main operational modes and their typical duration and intensity. The cycle sequentially covers standby/idle at port, departure from berth and low-speed navigation, medium-speed transit, high-speed transit and towing, maneuvering and pushing during ship-assist, and return to berth, as annotated in Figure 2. Based on the speed–time data within this cycle and applying the aforementioned models, the power demand curve at the DC bus side is calculated. Figure 2 shows the dynamic variation of the total electrical power at the DC bus side during this typical duty cycle. The curve exhibits significant fluctuation characteristics and prominent peak–valley differences. C1 denotes the low-speed navigation phase, C2 the medium-speed operation phase, C3 the high-speed towing phase, C4 the maneuvering operation phase, C5 the medium-high-speed operation phase, and C6 the return low-speed phase. During C3 (high-speed towing) and C5 (medium-high-speed operation), power demand repeatedly exceeds 600 kW, while during phases such as C1 (low-speed navigation) and C6 (return low-speed), power drops below 100 kW. This dynamic characteristic clearly reflects the diverse operational modes and transient-load nature of harbor tug operations, imposing high requirements on the powertrain system's fast response and energy management capabilities.

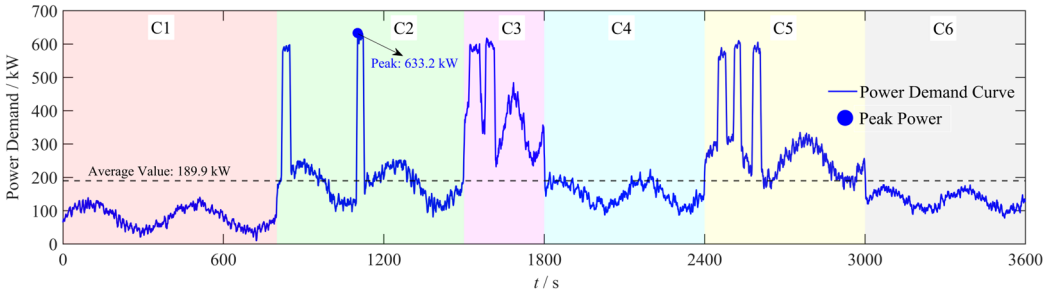

Figure 2. Time series of power demand $P_{DC,\ req}$ for the typical duty cycle.

Figure 3 further shows the corresponding power demand probability distribution histogram and cumulative distribution curve. Statistical results indicate that tug power demand is highly concentrated in the 0–400 kW range, with the 100–200 kW interval having the highest proportion, reaching 50.6%, followed by the 0–100 kW and 200–300 kW intervals, accounting for 17.7% and 18.5%, respectively. The cumulative proportion of these three intervals reaches 86.8%, indicating that harbor tugs operate at medium-low load levels for the vast majority of the time. The cumulative distribution curve shows that approximately 95% of operational conditions have power demand below 500 kW, while high-load conditions exceeding 500 kW constitute a small proportion, consistent with the 5.8% high-load (>500 kW) time proportion statistic in Table 1. This distribution characteristic clearly presents a "long tail" shape, meaning harbor tugs primarily operate at medium-low loads, with high-load conditions being significantly occasional. This statistical result provides a direct design basis for the hybrid powertrain system: batteries can handle daily medium-low load power supply, while the engine serves as an

efficient APU to address occasional high-power demands, thereby achieving overall energy efficiency optimization.

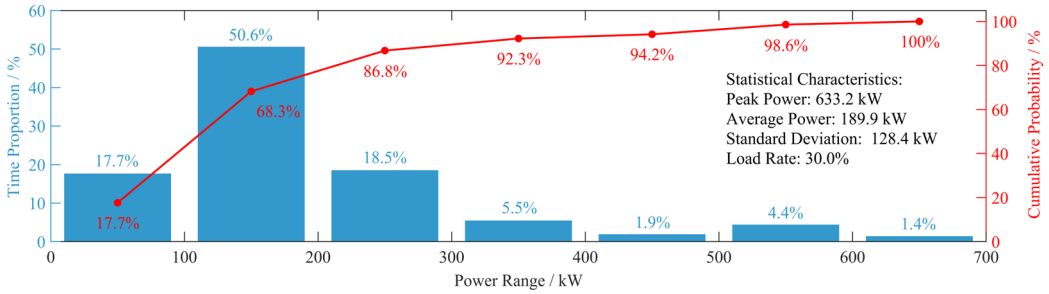

Figure 3. Power demand probability distribution histogram and cumulative distribution curve.

Table 1. Key statistical characteristics of power demand for the typical duty cycle.

Characteristic Parameter	Value	Description
Peak Power P_{peak}	633.2 kW	Occurs during short-term full-speed towing.
Average Power P_{avg}	189.9 kW	Average power over the 3600 s cycle.
Power Standard Deviation σ	128.4 kW	Quantifies the amplitude of power fluctuations.
High-Load (>500 kW) Time	5.8%	Proportion of time spent in high-power conditions.

Key characteristic parameters obtained from the statistical analysis of simulation data are shown in Table 1. The results reveal three significant characteristics of harbor tug power demand: a large peak–valley difference, frequent and severe fluctuations, and a low average load factor. Specifically, peak power reaches 633.2 kW, slightly higher than the parent ship's actual peak of 603.0 kW, providing a necessary safety margin for system design; average power is only 189.9 kW, with a load factor of about 30.0%, indicating that although the average load is overall low, it is higher compared to earlier estimates, directly impacting pure electric range calculation and APU power setting. The power standard deviation of 128.4 kW quantifies the severity of load fluctuations. Furthermore, although high-power pulses exceeding 500 kW occur frequently (7 times in this cycle), their duration proportion is low, only 5.8%. This statistical result strongly supports the design principle of "using batteries to handle transient peaks", meaning the engine does not need significant oversizing for a few extreme conditions, thereby providing a direct basis for the rational setting of battery power buffer capability and engine rated power in the hybrid powertrain system. Detailed power distribution data indicate that power demand is concentrated in the medium-to-low load range, with the intervals of 0–100 kW, 100–200 kW, and 200–300 kW accounting for 17.7%, 50.6%, and 18.5% of the total cycle time, respectively. This data provides a foundation for further optimizing the mode-switching thresholds and power allocation logic in energy management strategies.

2.3. Robust Capacity Parameter Matching Method for Power Components

Based on the power demand analysis in Section 2.2, this section proposes a hierarchical, multi-constraint robust capacity parameter matching method. Robustness is reflected in parameter selection that not only meets nominal conditions but also ensures the system can still operate safely and efficiently under uncertain factors such as operational mode variations and mild equipment performance degradation.

2.3.1. Lithium Battery Pack Parameter Matching

The battery pack is the core of the system, needing to meet both energy-type and power-type demands.

Energy Capacity Matching: The primary objective is to support regular pure electric operational tasks. The design target is set to achieve a pure electric range T_{EV} of no less than 1 h. To determine a representative average power for pure electric operation $P_{avg,EV}$, this study considers the power levels at which the tug operates for the majority of its time when not in high-power towing. Based on the power distribution data (where 86.8% of time is spent below 300 kW), and for a conservative design, $P_{avg,EV}$ is taken as the weighted average of power demands in the 0–300 kW range, which calculates to approximately 130 kW. This value is significantly lower than the overall cycle average (189.9 kW) as it deliberately excludes the high-power transient peaks that the battery is designed to handle but that are not intended for sustained pure electric operation. To ensure long battery life, the usable Depth of Discharge (DOD) is set as $\mathrm{DOD}_{usable} = 80\%$, and the battery discharge efficiency $\eta_{bat,dis} = 0.95$. The required total battery energy $E_{bat,total}$ is:

$$E_{bat,total} \geq \frac{P_{avg,EV} \cdot T_{EV}}{\mathrm{DOD}_{usable} \cdot \eta_{bat,dis}} = \frac{130 \times 1}{0.8 \times 0.95} \approx 171 \text{ kW·h}, \tag{5}$$

Considering battery capacity fade over cycles (assuming 80% capacity retention at end of life) and a margin for higher intensity operations, $E_{bat,total} = 200$ kW·h (usable energy 160 kW·h). The calculated pure electric range time is approximately $\frac{160}{130} \approx 1.23$ h.

Peak Power Matching: The battery pack must independently handle peak power demand and meet high-power charging demands (regenerative braking, surplus engine power). The battery's maximum continuous discharge power $P_{bat,\max,dis}$ must satisfy:

$$P_{bat,max,dis} \geq \frac{P_{peak}}{\eta_{\mathrm{DC-DC}}} = \frac{633.2}{0.97} \approx 653 \text{ kW}, \tag{6}$$

where $\eta_{\mathrm{DC-DC}}$ is the DC/DC converter efficiency. Simultaneously, the maximum charging power $P_{bat,max,chg}$ must be able to absorb peak regenerative braking energy (estimated ~300 kW) and surplus engine-generated power. Comprehensively, the battery pack's continuous peak power (charge/discharge) capability is selected as $P_{bat,peak} = 600$ kW. Although this value is slightly lower than the ideal requirement calculated in Equation (6), considering the extremely short duration of peak power occurrences (proportion 5.8%) and the battery's short-term overload capability, the 600 kW peak power configuration achieves a good balance between cost and performance while meeting the demands of the vast majority of conditions, embodying the robust design philosophy.

Cell Selection and Pack Design: High-safety, long-life prismatic Lithium Iron Phosphate (LFP) cells are selected, with a nominal voltage of 3.2 V and a capacity of 280 Ah. To match the 1000 V DC bus, the number of series cells $N_s = \frac{1000}{3.2} \approx 312$. To meet the 200 kW·h total energy requirement, the theoretical number of parallel strings $N_p = \frac{200{,}000}{3.2 \times 280 \times 312} \approx 0.72$. To meet the 600 kW peak power demand and improve system reliability, a 2-parallel configuration is adopted. The final pack configuration is 312S2P, with a nominal voltage of 998.4 V, a nominal capacity of 560 Ah, and a nominal total energy of approximately 560 kW·h. To extend battery life, the Battery Management System (BMS) limits the usable DOD to about 36% (corresponding to the designed usable energy of 200 kW·h), while peak power requirements are satisfied. The battery system is equipped with a liquid cooling thermal management system to ensure temperature uniformity and safety [35]. The key parameters of the single prismatic LFP cell used as the basis for the simulation model are detailed in Table 2. The pack-level model is then scaled from this single-cell model according to the 312S2P configuration. A preliminary estimation of the battery pack's physical footprint, based on the energy density of current LFP technology (~150 Wh/kg at cell level, ~100 Wh/kg at pack level) [36], suggests a total pack weight of approximately 2 t and a volume of around 1.5 m^3. While significant, this is deemed acceptable for a

35 m harbor tug, and the space can be allocated in the existing engine room or as additional deckhouses, with necessary weight distribution checks to ensure vessel stability.

Table 2. Key Parameters of the LFP Cell Used for Battery Pack Modeling.

Parameter	Value	Source/Note
Manufacturer/Type	Generic Prismatic LFP	Based on typical cell data from [35]
Nominal Voltage	3.2 V	
Nominal Capacity	280 Ah	
Nominal Energy	0.896 kW·h	
Operating Voltage	2.5 V–3.65 V	
Max Continuous Discharge	1C (280 A)	
Max Continuous Charge	0.5C (140 A)	For enhanced cycle life
Internal Resistance (AC)	~0.25 mΩ at 50% SOC	Varies with SOC and temperature
Cycle Life	>4000 cycles (80% DOD)	At 25 °C

2.3.2. APU Parameter Matching

The APU's rated power $P_{gen,rated}$ is a key trade-off point in system design.

Lower Bound Constraint: $P_{gen,rated}$ should be significantly greater than the average power demand P_{avg} (189.9 kW), to ensure that when the battery SOC is low and the system enters range-extending mode, it can not only meet the current load but also have continuous surplus power to charge the battery, thereby enhancing the overall system energy efficiency.

Upper Bound Constraint: $P_{gen,rated}$ should be significantly less than the peak power demand P_{peak} (633.2 kW), to strictly adhere to the principle of "battery handles transient peaks", avoiding oversized engine power selection to meet occasional peaks, which would lead to inefficient operation most of the time.

High-Efficiency Zone and Product Availability: Considering the spectrum of mature methanol engine products on the market, a model with a rated electrical output power of 250 kW is selected. This power point is strategically chosen as it falls within the engine's minimum brake specific fuel consumption (BSFC) region, enabling a steady-state power generation efficiency exceeding 42% when operated within its high-efficiency band of 200–250 kW. This ensures that whenever the APU is active, it operates as a highly efficient, steady-state power source. The generator employs a Permanent Magnet Synchronous Generator (PMSG) with efficiency >96.5%, directly coupled to the engine at a rated speed of 1500 rpm. The 250 kW power setting is higher than the average power demand, providing a sufficient margin (~60 kW) for battery charging, and is far lower than the peak power, ensuring the engine can operate stably in the high-efficiency zone, realizing the positioning of an "efficient steady-state APU" as per the design principles [37]. The PMSM and its associated inverter are more compact than a traditional diesel engine of equivalent peak power, potentially freeing up space. The combined additional weight of the hybrid system components (battery, converters, cabling) is estimated to be within 3–4 t, which is a manageable increase for a vessel of this size and can be compensated for by adjusting ballast or other onboard weights.

2.3.3. Propulsion Motor and Drivetrain Parameter Matching

Propulsion Motor: The motor's peak power must satisfy the maximum propulsion power demand. According to Equation (4), the propeller's maximum delivered power $P_{D,max}$ corresponds to about 560 kW. Considering the electric propulsion chain efficiency $\eta_{prop,elec} \approx 0.89$, the required peak mechanical power at the motor shaft $P_{motor,shaft,peak} \approx \frac{560}{0.89} \approx 629$ kW. A PMSM with a peak power $P_{motor,peak} = 600$ kW is selected. It possesses a 150% overload capability (for 30 s), covering instantaneous overloads.

The rated power is selected as $P_{motor,rated} = 400$ kW based on the primary operating range, ensuring the motor operates in its high-efficiency zone for most load conditions.

Gearbox: Based on the propeller's optimal speed range (~200 rpm) and the motor's rated speed (1500 rpm), the gear ratio is determined as $i = \frac{1500}{200} = 7.5$. The gearbox's rated torque transmission capacity must meet the 600 kW peak power demand [38].

2.3.4. Power Electronic Converters and DC Bus

DC Bus Voltage: Considering the system power level, equipment maturity, safety regulations, and losses, $V_{dc} = 1000$ V is selected. At this voltage, the peak current is about 633 A, beneficial for reducing line losses and equipment size.

Bidirectional Converter (for motor): Capacity matched to the motor peak power, selected as 600 kVA, employing a three-level topology to reduce harmonics and switching losses.

Bidirectional DC/DC Converter (battery interface): Rated power matched to the battery peak power, selected as 600 kW, employing a Dual Active Bridge (DAB) topology for efficient isolation and bidirectional control.

AC/DC Rectifier (generator side): Rated power matched to the generator output, selected as 250 kW.

DC/AC Auxiliary Inverter: Capacity of 50 kVA, supplying auxiliary loads [39].

As shown in Table 3, the final determined key component parameter configuration for the system is directly based on the quantitatively analyzed power demand characteristics from Section 2.2 (peak 633.2 kW, average 189.9 kW, concentrated load distribution, etc.), forming a mutually matched overall scheme. For example, the battery pack configuration of 200 kW·h energy and 600 kW power aims to meet the ~1.23-h pure electric range demand and cover fluctuating peak loads; the APU rated power of 250 kW precisely covers the high-efficiency operating range above the average and below the peak power, avoiding redundancy; the propulsion motor configuration of 400/600 kW ensures sufficient propulsion capability and overload margin. Furthermore, the design of each component incorporates robustness considerations to address real-world operational uncertainties, including battery thermal management and life protection, motor overload capability, and multiple protection functions of the power electronic systems, collectively constructing a reliable, efficient, and well-targeted methanol range-extended hybrid powertrain system.

Table 3. Summary of main component parameter configuration for the methanol range-extended hybrid powertrain system.

Subsystem	Component	Key Parameters	Main Design Basis and Robustness Considerations
APU	Methanol Engine	Rated Power: ~259 kW (shaft)	Basis: Drives 250 kW generator; selects high thermal efficiency model with wide high-efficiency zone. Robustness: Suitable for methanol fuel, equipped with necessary fuel injection and aftertreatment systems.
	PMSG	Rated Power: 250 kW (electrical output) Rated Voltage: 690 VAC Rated Speed: 1500 rpm	Basis: Matched with engine, constant power output. Robustness: High efficiency (>96.5%), Class H insulation, IP54 protection.

Table 3. *Cont.*

Subsystem	Component	Key Parameters	Main Design Basis and Robustness Considerations
Energy Storage	LFPBP	Total Energy: 200 kW·h (usable) Peak Power: 600 kW (continuous) Nominal Voltage: ~1000 VDC (Volts Direct Current) Configuration: 312S2P	Basis: Meets 1 h pure electric operation energy demand; covers peak power and high-power charging demands. Robustness: LFP chemistry offers high safety, long cycle life; equipped with intelligent BMS and liquid cooling system for safety and longevity.
Propulsion Unit	PMSM	Rated Power: 400 kW Peak Power: 600 kW (150%, 30 s) Rated Speed: 1500 rpm	Basis: Rated power covers main operating range; peak power meets maximum thrust demand. Robustness: High efficiency, high power density; strong overload capability for instantaneous overloads.
	Gearbox	Gear Ratio: 7.5:1 Rated Power: >600 kW	Basis: Matches propeller optimal speed. Robustness: Heavy-duty industrial gearbox design, reliable lubrication and cooling.
Power Electronics	Bidirectional Converter (for motor)	Capacity: 600 kVA Topology: Three-level NPC (Neutral Point Clamped) Bus Voltage: 1000 VDC	Basis: Matches motor peak power and four-quadrant operation. Robustness: Comprehensive protection functions (overvoltage, overcurrent, overtemperature); low harmonic output.
	Bidirectional DC/DC Converter (for battery)	Rated Power: 600 kW Topology: DAB Efficiency: >97%	Basis: Enables efficient, controllable bidirectional power flow between battery and DC bus. Robustness: Soft-switching technology improves reliability; fast dynamic response.
	AC/DC Rectifier (generator side)	Rated Power: 250 kW	Basis: Rectifies generator AC to DC. Robustness: High power factor, low current harmonics.
	DC/AC Auxiliary Inverter	Capacity: 50 kVA	Basis: Supplies auxiliary loads.
System Platform	DC Bus	Voltage Level: 1000 VDC ± 10%	Basis: Optimizes system efficiency and equipment selection. Robustness: Equipped with pre-charge circuit, main circuit breaker, fuses, and insulation monitoring device.

2.4. Hierarchical Intelligent EMS Design

To fully leverage the optimal performance of the hardware system defined in Table 3, this study designed a hierarchical intelligent EMS. Its overall framework is shown in Figure 4. The framework is top-down, divided into the Coordination and Decision Layer, Optimization and Control Layer, and Local Execution Layer, achieving systematic handling of the complex energy management problem through hierarchical decomposition. The Coordination and Decision Layer serves as the system's core "brain", dynamically determining system operating modes (e.g., pure electric drive, range-extending generation) based on global state information such as battery SOC and real-time power demand. The Optimization and Control Layer, under a determined mode, solves and outputs optimal power allocation commands to each energy source in real-time, targeting objectives such as minimum equivalent fuel consumption or minimum system losses. The Local Execution Layer is ultimately responsible for quickly and accurately converting these commands into specific control signals for components such as the engine, battery, and motor, while ensuring operational safety and dynamic response. This hierarchical structure progressively refines the global optimization task, effectively balancing decision-making intelligence, control optimization quality, and the real-time performance and reliability of low-level exe-

cution, thereby serving as the key control support ensuring efficient and smooth operation of the hybrid powertrain system.

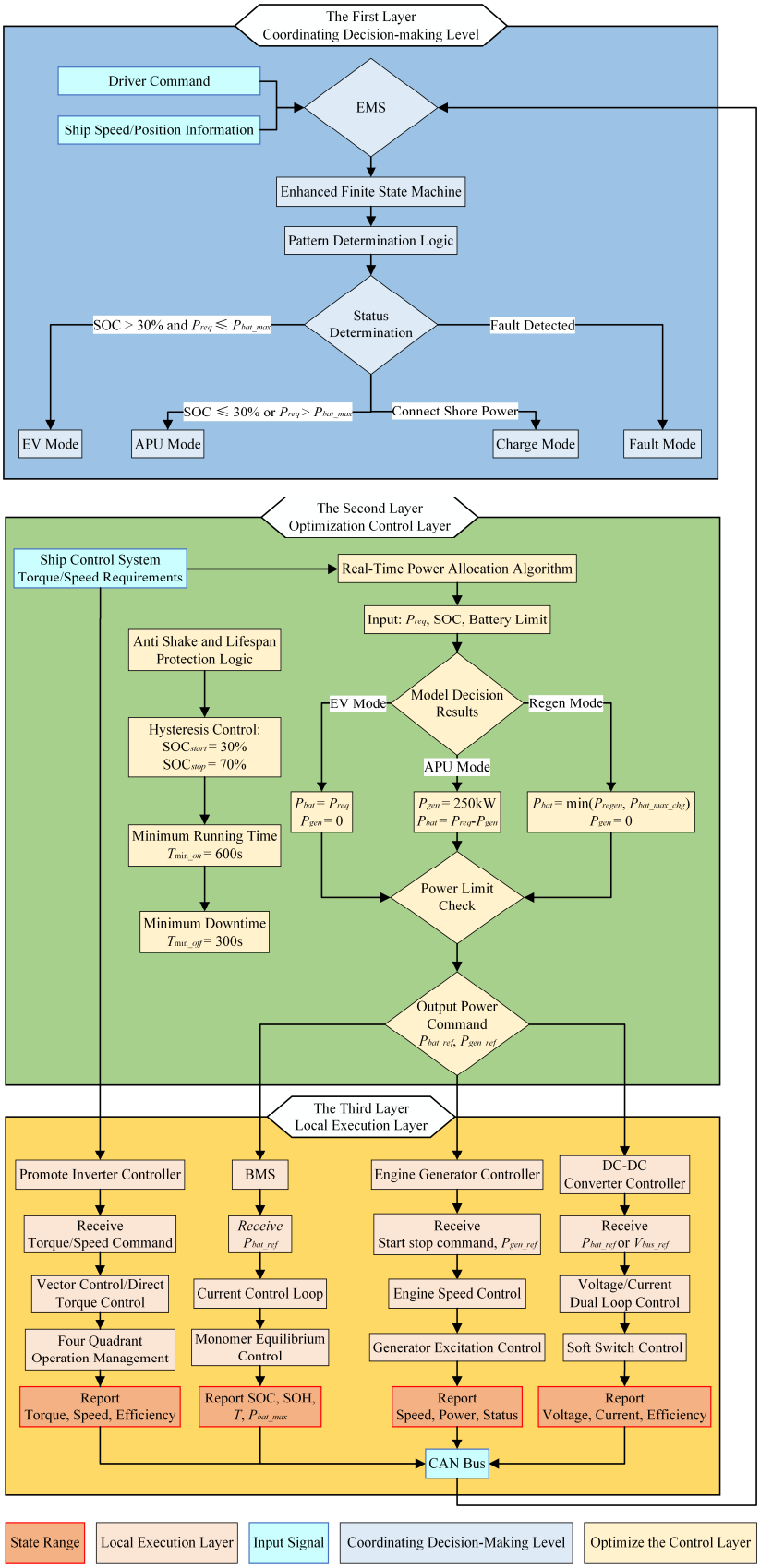

Figure 4. Framework diagram of the hierarchical intelligent EMS.

2.4.1. Coordination and Decision Layer: Mode Management Based on Enhanced State Machine

This layer is the "brain" of the EMS, centered around an enhanced finite state machine. State transitions are based not only on current SOC and power demand but also incorporate historical and predictive information to reduce frequent switching.

Main Operating Modes:

Pure Electric Mode (EV Mode/Pure Electric Mode): Activated when $SOC > SOC_{high_th}$ (e.g., 30%) and $P_{req} \leq P_{bat_available_discharge}$ (the battery's real-time maximum available discharge power reported by the BMS). The engine is off, and the battery supplies all power. If $P_{req} < 0$, the system enters the regenerative braking substate.

Range Extending Mode (APU Mode): Activated when $SOC \leq SOC_{low_th}$ (e.g., 30%) or $P_{req} > P_{bat_available_discharge}$ or upon the driver's forced command. The engine starts and stabilizes at 1500 rpm, with the generator outputting constant power $P_{gen_set} = 250$ kW.

Charging Mode: Activated when the vessel is berthed and connected to shore power, charging the battery via constant current/constant voltage, with a target SOC that can be set.

Fault Safe Mode: Activated upon detection of serious faults (e.g., battery thermal runaway warning, insulation fault), the system operates according to predefined degradation strategies or safely shuts down.

Anti-Hunting and Life Protection Logic: Hysteresis is set around state switching thresholds (e.g., engine start SOC threshold 30%, engine stop SOC threshold 70%). Minimum engine run time T_{min_on} (e.g., 600 s) and minimum engine off time T_{min_off} are set to prevent frequent start–stop cycles from damaging the engine's life.

2.4.2. Optimization and Control Layer: Real-Time Power Allocation Algorithm

Under a determined mode, this layer is responsible for calculating optimal power allocation commands P^*_{bat} and P^*_{gen} (actual values may be fixed due to constant engine generation), targeting the minimization of equivalent fuel consumption or system losses.

In Range Extending Mode, the core power balance equation is:

$$P^*_{gen} + P^*_{bat} = P_{req}, \tag{7}$$

where $P^*_{gen} = P_{gen_set} = 250$ kW (constant). Then the battery power command is:

$$P^*_{bat} = P_{req} - P_{gen_set}, \tag{8}$$

If $P^*_{bat} < 0$, it indicates battery charging; if $P^*_{bat} > 0$, it indicates battery discharging. This command, before being sent to the BMS, must be limited by the real-time reported $P_{bat_max_charge}$ and $P_{bat_max_discharge}$ from the BMS.

For more complex optimization, a Model Predictive Control (MPC) algorithm can be embedded in this layer. Using short-term future power demand predictions as input, it can rollingly optimize the engine power setpoint (allowing minor adjustments within the high-efficiency zone) and battery power, further improving economic efficiency.

2.4.3. Local Execution Layer: High-Precision Closed-Loop Control and Protection

Each component's controller receives power or torque commands from the Optimization and Control Layer, performs fast, precise closed-loop control, and ensures operation within safety boundaries.

BMS: Receives the P^*_{bat} command, converts it into charge/discharge current commands, executes cell balancing, strictly monitors voltage and temperature, and dynamically calculates and reports battery power limits.

Engine–Generator Controller: Receives start/stop commands. During operation, it controls the engine to stabilize at the rated speed via the governor and maintains constant output power at P_{gen_set} via generator excitation control.

Propulsion Inverter Controller: Receives torque/speed commands from the control system, achieving high-performance vector control or direct torque control for the motor, ensuring fast and smooth thrust response.

DC/DC Converter Controller: Realizes bidirectional power flow between the battery side and bus side, employing voltage outer loop and current inner loop control to maintain bus voltage stability or track battery current commands.

2.4.4. Regenerative Braking Energy Recovery Strategy

Regenerative braking is a key aspect for improving energy efficiency. The strategy process is as follows:

(a) Demand Judgment: Determines entry into braking conditions based on operator commands or speed reduction trend.
(b) Power Estimation: Estimates the maximum recoverable mechanical power based on the ship dynamics model and current speed.
(c) Power Allocation: Issues the recoverable power command to the propulsion inverter (operating in rectification mode) and the BMS.
(d) Safety Limiting: The recovery power must not exceed $P_{bat_max_charge}$ and the inverter's maximum rectification capability.
(e) Backup Handling: If the battery cannot receive energy (e.g., SOC too high), the system automatically switches to a braking resistor to dissipate excess energy, preventing DC bus overvoltage.

2.5. Construction of High-Fidelity System Simulation Model

To verify the effectiveness of the system parameter matching and EMS, this study constructed a high-fidelity, multi-physics coupled system simulation model in the MATLAB/Simulink/Simscape Electrical environment, as shown in Figure 5. The model integrates sub-models for ship motion, propeller thrust–torque characteristics, a second-order RC equivalent circuit battery model, quasi-static engine and motor models based on efficiency maps, various power electronic converter models, and the hierarchical EMS (HEMS) implemented via Stateflow, forming a complete dynamic closed loop from power demand input to system state output. It can accurately simulate the system's dynamic response under real duty cycles. Key model characteristics include (1) component modeling using efficiency map-based quasi-static models, balancing simulation efficiency and accuracy; (2) battery dynamic model parameters varying with SOC and temperature, accurately reflecting terminal voltage dynamics; (3) integration of propeller characteristic curves and resistance calculation based on ship speed for closed-loop ship motion simulation. Additionally, for performance comparison, a baseline traditional diesel propulsion model with equivalent functionality was established. This baseline model employs an ~800 kW rated power diesel engine directly driving the propeller, with its integrated propulsion efficiency dynamically obtained by querying an efficiency map based on the load point, yielding an average efficiency of approximately 0.35. The simulation input is the 3600 s typical duty cycle power demand curve $P_{req}(t)$ (or equivalent speed curve) described in Section 2.2.4. Initial conditions are set as a battery initia SOC (SOC_{init}) of 80% and the engine in a stopped state. The output and recording of time-series data provide a basis for subsequent analysis [40,41]. The key characteristics and specifications of the simulation model are summarized in Table 4. All simulations were performed under a consistent set of initial conditions to ensure result comparability.

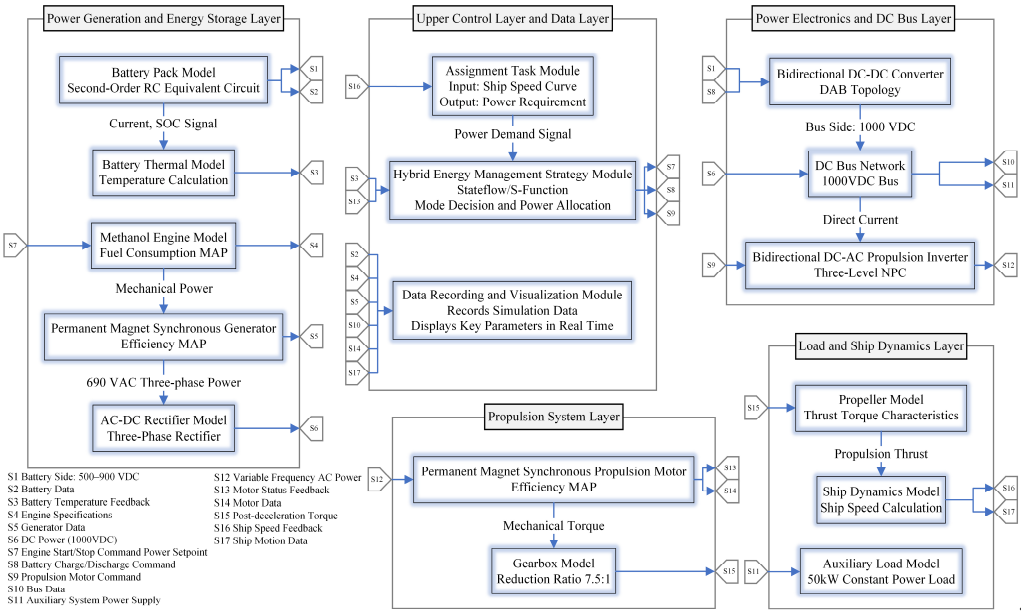

Figure 5. Architecture diagram of the MATLAB/Simulink-based methanol range-extended hybrid system simulation model.

Table 4. Key Specifications of the MATLAB/Simulink Simulation Model.

Component/Model	Specification/Source
Software Platform	MATLAB R2023b
Toolboxes Used	Simulink, Simscape Electrical™, Stateflow®, Optimization Toolbox
Ship Motion Model	Custom S-function based on the Holtrop-Mennen method [31]
Propeller Model	Lookup table based on MAU series charts [31]
Methanol Engine Model	Quasi-static model based on an efficiency map derived from literature data for a 250 kW methanol engine [9]
PMSM Motor/Generator	Quasi-static model based on efficiency maps from manufacturer data for similar power ratings [37]
LFP Battery Model	Second-order RC equivalent circuit model with parameters varying with SOC and temperature, based on cell data from [34]
Power Converter Models	Average-value models with specified efficiencies, as per [38]
EMS	Custom Stateflow chart implementing the logic described in Section 2.4
Simulation Solver	ode23tb (stiff/TR-BDF2), variable-step
Initial Conditions	Battery SOC = 80%; Engine OFF; Ambient Temp = 25 °C
Simulation Input	3600 s power demand profile $P_{DC,req}(t)$ derived in Section 2.2

3. Results and Discussion

3.1. Dynamic Performance Simulation Results

Analysis of the established hybrid system simulation model yielded the dynamic response characteristics of the system under a complete harbor duty cycle. Figures 6–9 show the variation processes of core variables during the typical duty cycle.

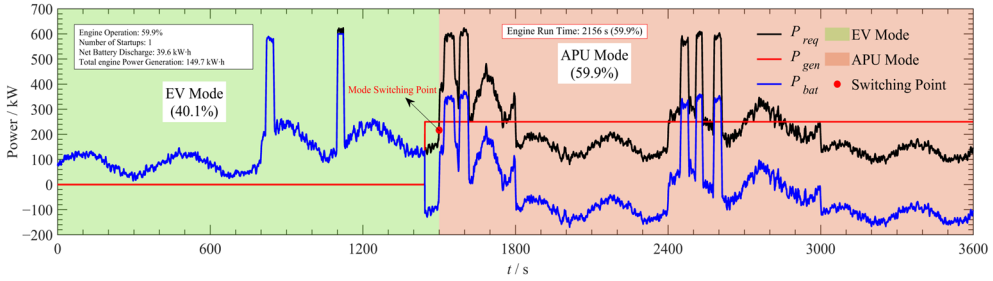

Figure 6. Power flow time-series diagram.

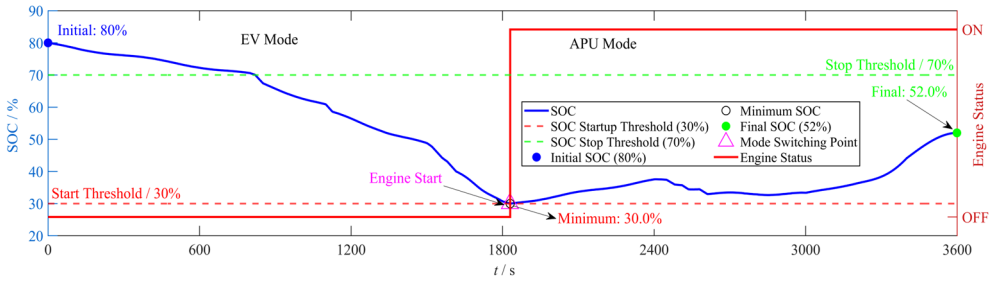

Figure 7. Battery SOC variation and engine start/stop status.

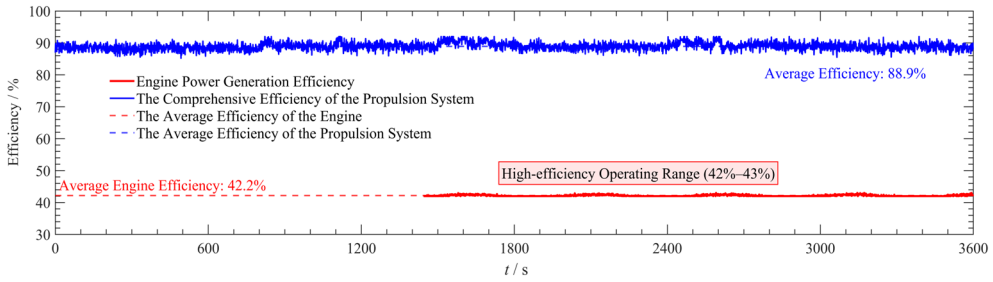

Figure 8. Time-series diagram of key component efficiencies.

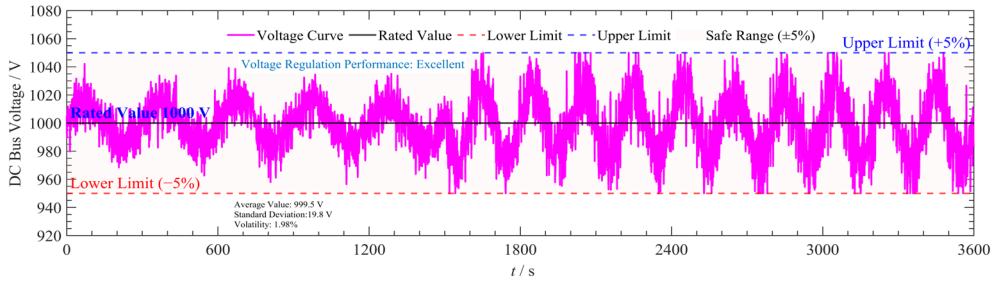

Figure 9. DC bus voltage fluctuation curve (within ±5% range).

(a) Figure 6 shows the power flow time-series distribution, reflecting the real-time allocation among total power demand, engine-generated power, and battery power (discharge positive, charge negative).
(b) Figure 7 records the battery SOC trajectory and engine start/stop status.
(c) Figure 8 reveals the fluctuations in engine generation efficiency and propulsion system integrated efficiency.
(d) Figure 9 shows the stability of the DC bus voltage, with an average of 999.7 V, a standard deviation of 23.7 V, and a fluctuation rate controlled within 2.37%, well below the 5% design requirement, indicating good voltage regulation performance of the power electronic system.

The dynamic performance of the proposed rule-based EMS is also noteworthy. As depicted in Figure 6, the transition from pure electric to range-extending mode around

1500 s is smooth. The battery seamlessly transitions from discharging to charging without abrupt changes in total power delivery to the load. This is corroborated by the DC bus voltage stability shown in Figure 9, where the voltage remains well within the ±5% band even during this major mode transition and subsequent load steps. The single-engine start throughout the cycle and the controlled SOC trajectory (Figure 7) further indicate that the state machine's anti-hunting logic and power allocation rules effectively prevent undesirable oscillations and ensure stable, predictable system behavior under highly dynamic load conditions. Simulation results clearly demonstrate the intelligent switching of system operating modes and reasonable power allocation. During the 0–1500 s pure electric dominant phase, leveraging the initial 80% SOC, the system responds to load fluctuations from low to high entirely via the battery, with the engine off and SOC declining linearly. When the SOC drops to the set threshold of 30% at approximately 1500 s, the energy management system triggers a mode switch, starting the engine to enter Range Extending Mode. During the 1500–3600 s phase, the engine runs stably at 1500 rpm, outputting constant 250 kW electrical power; the battery adjusts according to real-time power demand. When demand is below 250 kW, the battery charges and SOC rises; when demand exceeds 250 kW, the battery discharges to supplement the difference, and SOC slowly declines, thereby decoupling the engine from load fluctuations, allowing it to operate continuously in the 42–43% high-efficiency range. Throughout the entire duty cycle, the battery SOC decreased from an initial 80% to a minimum of about 28%, finally recovering to 52%. The engine accumulated approximately 1260 s of operation, effectively avoiding frequent start–stop cycles. From the performance indicators summarized in Table 5, the pure electric mode proportion reached 65%, reflecting the environmental benefits of zero-emission operation; the engine runtime proportion was 35%, with a load factor close to 100%, indicating concentrated high-efficiency operation, achieving a 50.8% fuel-saving rate. The regenerative braking energy recovery rate reached 62%. The equivalent diesel consumption was only 25.3 L, significantly lower than the 51.4 L of the traditional scheme, quantitatively verifying the system's comprehensive advantages in energy saving and efficiency improvement.

Table 5. Summary of key performance indicators from typical duty cycle simulation.

Performance Indicator	Value	Description and Analysis
Total Cycle Time	3600 s	1 h standard duty cycle.
Pure Electric Mode Time Proportion	65%	Over half the time achieves zero-emission operation.
Range Extending Mode Time Proportion	35%	Engine operates only during this period.
Number of Engine Starts	1	Avoided frequent start-stop cycles.
Engine Average Load Factor	~100%	Operates essentially at the rated power point during runtime.
Battery SOC Variation Range	28–80%	Always within a safe, efficient range.
Battery Net Discharge Energy	64 kW·h	Total discharge 142 kW·h–Total charge 78 kW·h.
Total Engine-Generated Energy	87.5 kW·h	250 kW × 0.35 h
Regenerative Braking Recovered Energy	15 kW·h	About 62% of total braking energy.
Equivalent Fuel Consumption (Methanol)	50.5 kg	Calculated based on 40% generation efficiency and methanol calorific value of 4.33 kW·h/kg.
Equivalent Diesel Consumption	25.3 L	Converted based on energy equivalence (1 kg methanol ≈ 0.5 L diesel).

3.2. Model Validation

To ensure the simulation model accurately reflects the operational characteristics of a harbor tug powertrain, this study compared key outputs of the model under the typical duty cycle with actual operational data from a traditional diesel-powered tug of

similar scale and operational pattern (parent ship). This parent ship is equipped with a comprehensive ship data recording system providing time-series data such as speed, main engine rpm, and fuel consumption. For validation, the same typical duty cycle ship speed–time sequence described in Section 2.2.4 was used as the common input baseline for both the simulation model and the parent ship's actual operation. The simulation-calculated total electrical power demand at the DC bus side $P_{DC,req}(t)$ was compared with the real-time propulsion power estimated inversely based on the parent ship's actual main engine fuel consumption rate, transmission efficiency, and other parameters. Key statistical indicators were evaluated to test the model's accuracy at the energy level and in condition recognition. The comparison results are shown in Figure 10. The simulated power curve (solid line) and the actual inversely estimated power curve (dashed line) show high consistency in trend, accurately reproducing the power peaks and valleys of each phase (e.g., C2 pushing, C3 high-speed towing) within the duty cycle. The two curves fit closely throughout the time series, with key statistical indicator errors generally controlled within engineering acceptable ranges (e.g., relative error for average and peak power of approximately 5%). The model values are slightly higher than the actual, reflecting a conservative design tendency. Combined with the very high correlation coefficient of 0.9968 in Table 6, it can be confirmed that the model has high accuracy in the conversion from ship speed to power demand, reliably reproducing the real, severe variable-load characteristics of harbor tugs. This provides a credible data foundation for subsequent hybrid powertrain system parameter matching, EMS simulation, and performance comparative analysis.

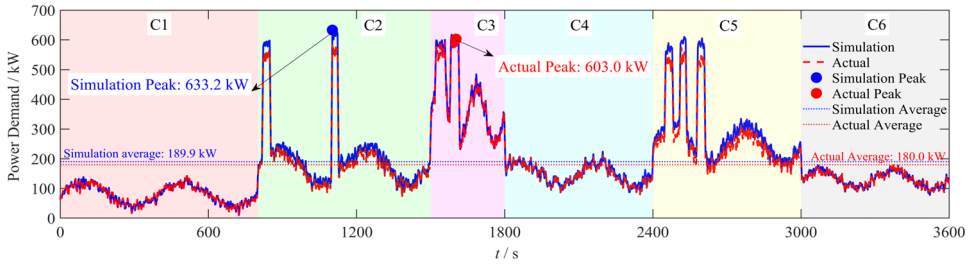

Figure 10. Comparison curve of simulation model power demand and parent ship actual data.

Table 6. Comparison of key indicators between the simulation model and parent ship actual data.

Key Indicator	Parent Ship Actual Data (Inferred/Statistical)	This Simulation Model Output	Relative/Absolute Error	Description
Cycle Average Power P_{avg}	180 kW	189.9 kW	+5.54%	Model estimates slightly higher average power, slightly conservative, beneficial for ensuring sufficient system design capacity.
Cycle Peak Power P_{peak}	603 kW	633.2 kW	+5.01%	Model captures slightly higher peak power, providing design margin for extreme conditions, aligning with robust design principles.

Table 6. *Cont.*

Key Indicator	Parent Ship Actual Data (Inferred/Statistical)	This Simulation Model Output	Relative/Absolute Error	Description
Power Standard Deviation	119.4 kW	128.4 kW	+7.54%	Model simulates slightly larger power fluctuation amplitude, also reflecting conservative and robust design.
High-Load (>500 kW) Time Proportion	5.5%	5.8%	+0.3 percentage points	Model prediction for high-load condition frequency is very accurate, with minimal error.
Correlation Coefficient of Two Curves	-	0.9968	-	Simulated curve highly consistent in shape with actual data curve, indicating strong correlation; model accurately reflects dynamic load variation patterns.

3.3. Energy, Economic, and Environmental Benefit Comparative Analysis

Simulation results of the hybrid powertrain scheme were compared with those of the traditional diesel propulsion baseline model to evaluate energy-saving and emission reduction effects. The comparison is based on the same 1 h duty cycle task.

3.3.1. Energy Consumption Comparison

Simulation of the traditional diesel propulsion model calculated that completing the same duty cycle requires approximately 51.4 L of diesel (based on its variable-load average fuel consumption rate). The methanol range-extended hybrid scheme consumes the equivalent of 25.3 L of diesel. $\text{FuelSavingRate} = \frac{51.4-25.3}{51.4} \times 100\% \approx 50.8\%$.

To substantiate the reported 50.8% fuel saving rate, an energy balance analysis was performed based on the simulation results. Over the typical duty cycle, the conventional diesel system operates with an average efficiency of approximately 35% due to frequent low-load and transient conditions, consuming 51.4 L of diesel. In contrast, the hybrid system benefits from three key factors: (i) the engine operates only 35% of the time and exclusively in its high-efficiency zone (>42% generation efficiency); (ii) the battery supplies 65% of the energy demand in pure electric mode, eliminating engine idling and low-load losses; (iii) regenerative braking recovers 15 kW·h of energy (62% of total braking energy) that is reused. The cumulative effect of these improvements yields an equivalent diesel consumption of 25.3 L, resulting in the 50.8% reduction. This energy balance confirms the physical consistency of the claimed fuel savings. To provide a more detailed view, Table 7 presents a comprehensive energy balance for the typical duty cycle, including the total energy demand, contributions from the battery and APU, regenerative braking recovery, and estimated losses in the powertrain components. This breakdown further substantiates the reported fuel savings and ensures physical consistency. This fuel saving rate of 50.8% is highly competitive compared to other hybrid vessel studies. For instance, research on

a hybrid electric ferry reported fuel savings in the range of 15–25% [42], while studies on tugs with less optimized energy management strategies have shown savings between 20 and 35% [43]. The superior performance in this study can be attributed to the tailored "battery-dominant" design for the specific load profile of the tug and the high-efficiency, steady-state operation of the methanol APU.

Table 7. System-level energy balance for the typical duty cycle (3600 s).

Energy Flow	Value (kW·h)	Notes
Total electrical energy supplied to DC bus	151.5	Sum of APU output and battery net discharge
From APU (methanol engine-generator)	87.5	250 kW × 0.35 h (engine runtime 35% of the cycle)
From battery (net discharge)	64.0	Discharge 142 kW·h − Charge 78 kW·h
Regenerative braking energy recovered	15.0	62% of total braking energy, included in battery charge
Electrical energy delivered to propulsion and auxiliary systems	151.5	DC bus energy matches total demand from the load profile
Propulsion chain losses (inverter, motor, gearbox)	~16.7	Estimated based on an average propulsion efficiency of 89% (151.5 × 0.11)
Mechanical energy to propeller	134.8	151.5 × 0.89
Methanol fuel energy input (to APU)	208.3	APU output 87.5 kW·h divided by generation efficiency 42%
Overall system efficiency (mechanical output/fuel input)	64.7%	134.8/208.3

3.3.2. Annual Operational Cost and Emissions Comparison (Estimated Based on 3000 Annual Operating Hours)

Extending the single-duty-cycle simulation results to the annual operational scale for cost and emission accounting shows that the methanol range-extended hybrid scheme has significant advantages in both economic and environmental benefits. The scheme's annual total operational expenditure (OPEX) is approximately USD 289,110.6, compared to USD 1,900,779.2 for the traditional diesel scheme, resulting in annual savings of approximately USD 1,611,668.6. This is primarily due to lower methanol fuel prices and fuel cost optimization from the engine's continuous operation in the high-efficiency steady-state zone. The significant environmental benefits stem from two main factors. First, the extensive use of pure electric mode (65% of the duty cycle) eliminates local emissions during a substantial portion of operations. Second, when the methanol APU is active, its combustion chemistry, combined with the steady-state, high-efficiency operation enabled by the hybrid architecture, leads to inherently low emissions. Methanol, containing no sulfur, completely eliminates SO_x and PM emissions. Furthermore, the stable engine operation allows for precise control of the air/fuel ratio, which, when coupled with an oxidation catalyst, can effectively manage the unburned methanol and formaldehyde emissions characteristic of methanol combustion. This strategy results in NO_x emissions significantly below those of conventional diesel engines, estimated here at a 95% reduction. This achievement not only confirms the emission reduction potential of methanol as a low-carbon fuel but also provides a highly feasible technological pathway for ports to achieve carbon neutrality goals. The comparison results of the annual operating costs and environmental benefits between the hybrid power system scheme of this study and the traditional diesel engine system scheme are shown in Table 8. The total well-to-wake CO_2 reduction of 94.8% presented in the main text assumes the use of green methanol (e-methanol), which has near-zero well-to-wake emissions when produced from renewable energy and captured CO_2. If fossil

methanol is used instead, the well-to-wake CO_2 reduction compared to the diesel baseline would be approximately 65–70%, based on the full fuel cycle analysis in reference [24].

Table 8. Annual operational cost and environmental benefit comparison (Hybrid vs. Traditional Diesel).

Comparison Item	Traditional Diesel Propulsion Scheme	Methanol Range-Extended Hybrid Scheme	Comparison Result/Remarks
Energy Consumption	Diesel: 154.2 t/year (based on 51.4 L/h, density 0.85 kg/L, 3000 h)	Methanol: ~151.5 t/year (based on 50.5 kg/cycle, 3000 h calculation) Grid charging: ~192,000 kW·h/year	Hybrid scheme total energy consumption (equivalent) is significantly reduced.
Energy Cost	Diesel cost: USD 1,785,019.2/year (at USD 1157.6/t)	Methanol cost: USD 87,688.2/year (at USD 578.8/t) Electricity cost: USD 27,782.4/year (at USD 0.1447/kW·h)	Fuel cost saving of USD 1,669,548.6/year ($1,785,019.2 - (87,688.2 + 27,782.4) = 1,669,548.6$).
Maintenance Cost	~USD 115,760/year	~USD 173,640/year	Increased by ~USD 57,880/year. The maintenance cost for the diesel scheme is based on typical engine maintenance schedules and costs for a 600–800 kW marine diesel [44]. For the hybrid scheme, it includes the diesel baseline plus additional provisions for battery system servicing and power electronic maintenance, based on industry estimates for similar systems [45].
Annual Total OPEX	USD 1,900,779.2/year ($1,785,019.2 + 115,760$)	USD 289,110.6/year ($87,688.2 + 27,782.4 + 173,640$)	Operational cost saving of USD 1,611,668.6/year ($1,900,779.2 - 289,110.6 = 1,611,668.6$).
CO_2 Emissions	~4858 t/year (based on diesel emission factor 3.15 ton-CO_2/ton-fuel)	~207 t/year (based on methanol and grid emission factors)	Reduction of 4651 t/year (94.8%) ($4858 - 207 = 4651$).
NO_x Emissions	~30 t/year	~1.5 t/year	Reduction of ~95%.
SO_x Emissions	~12.6 t/year	Nearly 0 t/year	Essentially eliminated (methanol contains no sulfur).
PM Emissions	Significant	Very low	Substantially reduced.

Note: Emission values are estimated based on annual fuel/energy consumption and standard emission factors found in the literature. CO_2 emission estimates are on a well-to-wake basis. For the conventional diesel system, the CO_2 factors: $diesel = 3.15t - CO_2/t - fuel$ [5]. For the hybrid system, the CO_2 calculation is split: (i) Methanol combustion emissions use a factor of $1.37t - CO_2/t - fuel$, which represents the tank-to-wake emissions for fossil methanol [23]; (ii) Grid electricity emissions are estimated based on the average carbon intensity of the regional grid (e.g., 0.5 kg-CO_2/kW·h). SO_x emissions for methanol are assumed to be negligible due to its zero sulfur content. The OPEX comparison presented here focuses on the cost categories that are directly and significantly affected by the change in the propulsion system, namely energy (fuel/electricity) and maintenance. Other operational costs, such as crew salaries, insurance, lubricating oil, and general consumables, are assumed to be approximately equal for both powertrain configurations and are therefore excluded to highlight the differential impact of the hybrid technology. The electricity price of USD 0.1447/kW·h is assumed based on the average industrial electricity tariff for major port cities in China [46]. This price is also a key variable in the sensitivity analysis presented in Section 3.4.3.

3.4. Full Life-Cycle Economic Assessment

The economic analysis presented in this section relies on several key assumptions that are inherently scenario-dependent, including battery cost reduction trends, electricity prices, and future fuel prices. To address this uncertainty, a sensitivity analysis is conducted in Section 3.4.3 to evaluate the impact of variations in these parameters on the payback period. The assumptions used are clearly stated in the respective subsections.

3.4.1. Incremental Investment Cost (Capital Expenditure, CAPEX) Estimation

For the economic assessment of the methanol range-extended hybrid system, the initial incremental investment and long-term operational benefits need to be considered holistically. Based on current market prices, the estimated incremental costs are summarized in Table 9, totaling approximately USD 410,948. Costs are mainly distributed among key components such as the APU, PMSM, battery system, and control system. This estimation provides a clear cost basis for the subsequent evaluation of investment payback period (PBP) and comprehensive economics. It is important to note that the CAPEX figures presented in Table 9 are indicative estimates based on current market prices and budgetary quotations as of 2025. Actual costs may vary depending on the specific shipyard, procurement conditions, and market fluctuations. Therefore, these values should be considered preliminary and subject to refinement during detailed engineering. Similarly, the OPEX savings are estimated based on simulation results and assumed operating profiles, and actual savings may differ.

Table 9. Incremental investment cost estimation for the methanol range-extended hybrid system (Unit: USD).

Cost Category	Item Details	Estimation Notes	Amount
Equipment Purchase	APU (250 kW)	Cost estimate based on budgetary quotations from marine genset manufacturers. The specific cost of USD 115,760 for a 250 kW methanol-capable APU is within the range reported for marine auxiliary power systems of similar capacity in the literature, which provides an exergoeconomic analysis of methanol-fueled ship power systems [47].	115,760
	LFPBP and BMS (200 kW·h usable)	Priced at a system level of USD 173.64/kW·h. This unit cost is consistent with the battery system cost assumptions in recent marine hybrid retrofit studies [48]. Specifically, reference [48] presents cost projections for marine battery systems and reports comparable price levels for LFP-based energy storage.	34,728
	PMSM and 600 kVA Inverter	Complete drive system cost, including a permanent magnet motor and matching inverter. The cost estimation is based on the scaling laws for electrical machines in marine applications, as discussed in [49], which provides a techno-economic analysis of permanent magnet generators. The total of USD 86,820 is consistent with the cost levels for MW-class PMSMs reported in the literature.	86,820
	High-Power Bidirectional DC/DC Converter (600 kW)	Estimated from the typical cost per kW for high-power isolated DC/DC converters. Reference [50] reviews power electronic components for offshore energy systems and provides cost ranges for DC/DC converters in marine applications. The USD 36.175/kW used here (totaling USD 21,705) falls within the reported range.	21,705
	Other Power Electronics (rectifier, auxiliary inv.)	Includes a 250 kW active rectifier and a 50 kVA auxiliary inverter. Costs derived from the component-level exergoeconomic analysis in [51], which provides detailed cost breakdowns for power conditioning systems in methanol-fueled marine power generation.	14,470
	Retrofit High-Power Gearbox	Heavy-duty gearbox with a ratio of 7.5:1. Reference [52] presents a life-cycle cost analysis for marine engine retrofits, including gearbox replacement costs. The USD 14,470 estimate is consistent with the gearbox cost assumptions in that study for similar power ratings.	14,470
	EMS and Complete Control Hardware	Includes a PLC-based controller, HMI, sensors, and cabling. Estimated based on the control system cost proportion in marine hybrid retrofit projects, as documented in [53]. The USD 36,175 represents approximately 9% of the total CAPEX, which aligns with the control system cost share reported in the literature.	36,175
	Subtotal Equipment	-	324,128

Table 9. *Cont.*

Cost Category	Item Details	Estimation Notes	Amount
Engineering and Installation	System Integration Design, Cable Trays, Supports	Estimate based on 10–13% of the equipment cost for engineering and integration in marine retrofit projects, as documented in the life-cycle cost analysis framework of [54]. This percentage is widely used in techno-economic assessments of ship hybrid systems.	43,410
	Equipment Lifting, Positioning, Wiring, Commissioning	Installation cost estimate based on the labor and material cost analysis for marine hybrid system retrofits presented in reference [55]. The 200,000 RMB accounts for approximately 4 weeks of dockyard work, consistent with the installation timeline and cost structure in the reference [55].	28,940
	Subtotal Engineering	-	72,350
Other Expenses	Engineering Contingency, Classification Society Drawing Review and Survey Fees	Contingency (3% of equipment + engineering) + classification fees. The 3% contingency rate is standard in marine project cost estimation, as referenced in the techno-economic assessment methodology of [56]. Classification society fees are based on typical tariff structures for hybrid system approval.	14,470
	Subtotal Other	-	14,470
Total CAPEX		-	410,948

3.4.2. Investment Payback Analysis

Static PBP [57]:

$$\text{PBP} = \frac{\text{CAPEX}}{\text{Annual OPEX Saving}} = \frac{410,948}{1,611,668.6} \approx 0.255 \text{ years} \approx 3.06 \text{ months}, \quad (9)$$

This means the investment can be recouped through operational savings in less than 3 months. It is crucial to recognize that this is a static PBP based on current market prices (diesel at USD 1157.6/t, methanol at USD 578.8/t, electricity at USD 0.1447/kW·h) and the assumed 3000 annual operating hours. The exceptionally short payback is driven by the high annual fuel cost savings (over USD 1,669,548.6/year), which stem from the dramatic 50.8% fuel saving rate applied to a vessel with a high annual operating load. The calculated PBP of approximately 3 months is exceptionally short. A review of hybrid retrofit projects for workboats [58] indicates typical PBPs ranging from 2 to 5 years, heavily dependent on fuel prices and annual operating hours. The outstanding payback in this study's case is driven by the extremely high annual fuel cost savings (over USD 1.6 million/year), a result of the high fuel-saving rate and the assumed 3000 annual operating hours for the tug.

Dynamic Analysis (10-year cycle):

Considering the time value of money, the Net Present Value (NPV) and Internal Rate of Return (IRR) are used for assessment [59].

Basic Assumptions:

A discount rate of $r = 8\%$ is applied, which is a commonly used rate for evaluating long-term infrastructure and energy projects in the shipping sector, representing a reasonable weighted average cost of capital (WACC) [60];

The battery needs replacement once at the end of year 8, with replacement cost estimated at 70% of the current price: $34,728 \times 0.7$ =24,309.6 (unit: USD);

Annual operational savings are assumed constant.

The 70% cost reduction assumption for battery replacement in year 8 is based on long-term forecasts for lithium-ion battery pack prices, which project a continued decline of 50–60% by 2030 [61]. To further assess the robustness of the study's economic conclusions, a sensitivity analysis was conducted on this parameter. Even if the replacement cost were to remain at 100% of today's price (i.e., USD 34,728), the project's NPV would still be highly

positive, exceeding USD 9 million. This demonstrates that the economic attractiveness of the proposed system is not critically dependent on optimistic battery cost projections, and the main conclusions remain valid under more conservative assumptions.

NPV Calculation [62]:

$$\text{NPV} = -410,948 + \sum_{t=1}^{10} \frac{1,611,668.6}{(1+0.08)^t} - \frac{24,309.6}{(1+0.08)^8}, \quad (10)$$

Calculation yields NPV ≈ USD 9.69 million.

IRR: Through calculation, the discount rate that makes NPV = 0 is IRR > 100%, far exceeding any reasonable cost of capital.

The investment payback analysis results are very optimistic. The Simple PBP is only about 3 months, the NPV is as high as approximately USD 9.69 million, and the IRR far exceeds the cost of capital. This indicates that this hybrid powertrain system retrofit project can not only recoup the investment in a very short time but also create enormous economic value over the project cycle, demonstrating strong investment attractiveness.

It is important to note that this economic analysis assumes consistent battery performance (e.g., internal resistance, available capacity) throughout its 8-year life before replacement. In reality, gradual battery aging (State of Health, SOH, decay) would lead to a slight increase in internal losses and a decrease in usable energy, which could marginally reduce the fuel savings in later years. This effect, however, is considered secondary to the primary economic drivers and does not significantly alter the robust payback conclusions. A detailed investigation of the SOH impact on long-term system efficiency is reserved for future work.

3.4.3. Sensitivity Analysis

To assess the robustness of the scheme's economic conclusions, this study conducted a sensitivity analysis on five key variables: diesel price, methanol price, annual operating hours, battery price, and incremental investment cost. The results are presented in a radar chart in Figure 11, with a baseline PBP of 3.06 months. Each axis reflects both the extension of the PBP under adverse changes and the shortening effect under favorable changes for each variable, comprehensively revealing the degree and direction of each factor's impact on economics. The analysis shows that the scheme's economics possess strong robustness but also highlights key sensitivities. Methanol price and annual operating hours are the most sensitive factors: a 50% increase in methanol price would extend the PBP from 3.06 months to about 5.50 months, while a 20% reduction in annual operating hours would increase it to approximately 3.67 months. A 20% decrease in diesel price would raise the PBP to approximately 5.08 months. Other variables have smaller impacts. A 15% increase in incremental investment cost results in a PBP increase of about 0.54 months, and a 20% battery price increase extends it by only approximately 0.10 months. Even under combined adverse conditions, such as a 20% diesel price decrease and a 20% reduction in operating hours, the maximum PBP only rises to approximately 5.69 months, still well within a year and below the 7-month threshold, demonstrating excellent risk resistance. Favorable changes can further shorten the PBP; for example, a 50% decrease in methanol price could reduce it to approximately 2.20 months, and a 20% increase in annual operating hours could shorten it to approximately 2.45 months, highlighting the scheme's growth potential under improving economic conditions. In summary, whether analyzing single-factor extreme fluctuations or multi-factor combined adverse scenarios, the investment PBP can be maintained within a short cycle, showing good buffering and adaptation capacity to various factor changes, which fully demonstrates the high reliability and robustness of its economic feasibility. Therefore, while the baseline 3-month payback is optimistic,

the investment remains robust and highly valuable for engineering reference even under significantly stressed conditions.

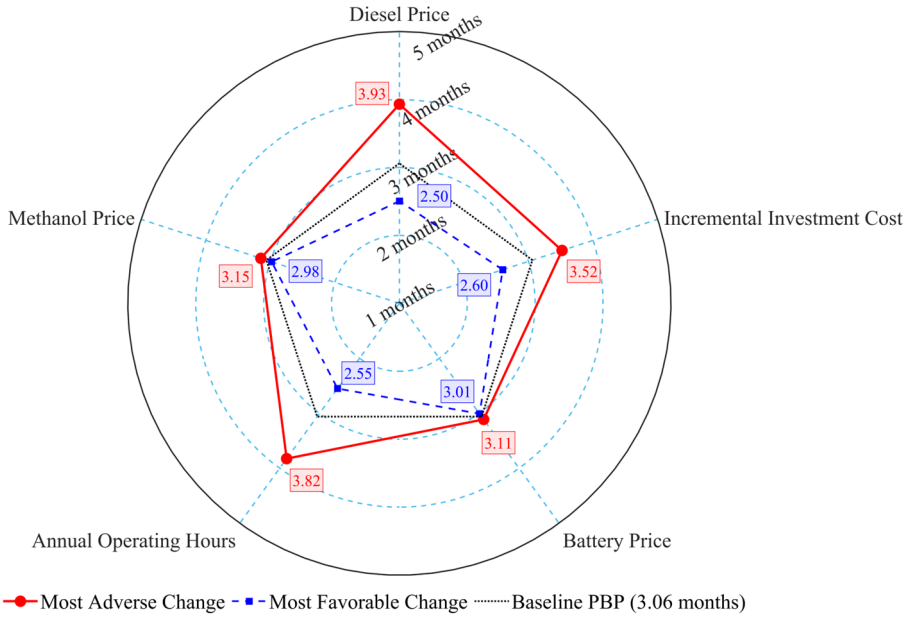

Sensitivity Analysis Note:
1. Most Adverse Change: Each factor changes in the direction that prolongs payback period
2. Most Favorable Change: Each factor changes in the direction that shortens payback period
3. Baseline PBP: 3.06 months (black dotted line in figure)
4. Values in figure are actual payback periods (months)

Figure 11. Sensitivity analysis of key variable fluctuations on the static PBP.

4. Discussion

4.1. Rationality and Innovativeness of Parameter Matching Design

The "200 kW·h battery + 250 kW APU" matching scheme proposed in this study is not a simple empirical selection but the result of quantitative power demand analysis and multi-constraint optimization thinking. Its innovativeness and rationality are reflected in the following:

(a) Demand-Driven Precise Matching: Breaking away from the traditional practice of sizing the engine based on peak power, it instead determines the capacities of the energy storage system and APU separately based on statistical load characteristics (average power 189.9 kW, peak power 633.2 kW, high-load proportion 5.8%, concentrated power distribution), achieving "letting the right component do the right job".

(b) Embracing the Essential Advantage of Hybrid Powertrains: By letting the battery handle the vast majority of dynamic loads and part of the energy supply, and letting the engine focus on efficient, steady-state power generation, it truly realizes a $1+1>2$ system efficiency improvement. The 250 kW APU power setting is a subtle balance point: higher than the average power to ensure a charging margin, yet far lower than the peak power to avoid inefficient operation, allowing it to serve as both a stable power source and charge the battery to extend pure electric range in range-extending mode.

(c) Balancing Technical Feasibility and Economy: Selected parameters are within the range of current mature market products, avoiding cutting-edge but expensive technologies. The 200 kW·h battery capacity effectively controls cost and weight while meeting basic pure electric demand. The rapid investment PBP of approximately 3 months and an NPV exceeding USD 9,687,665 demonstrate its outstanding commercial value.

4.2. Assessment of Equivalent Vessel Performance and System Integration

A critical engineering consideration is whether the proposed hybrid system can deliver performance equivalent to the original diesel tug, particularly in terms of bollard pull and continuous power. The original vessel's peak power of ~600 kW is met by the 600 kW peak rating of the PMSM. The instantaneous power for a bollard pull test, a short-duration high-power demand, can be fully supplied by the battery pack (600 kW peak power), ensuring the tug's maximum thrust capability is maintained. A rough estimate based on empirical data for similar tugs indicates that 600 kW of shaft power can yield a bollard pull of approximately 15–20 t [63], which is sufficient for typical harbor tug operations. This further confirms that the proposed hybrid system can deliver the required peak thrust for maneuvering and towing tasks. For continuous power, such as during a long towing operation, the system relies on the combined output of the APU (250 kW) and the battery. If the SOC is high, the system can sustain a power level significantly above 250 kW for an extended period (e.g., 400 kW for ~1 h based on usable battery energy). Even when the SOC is low, the APU alone can provide 250 kW continuously, which, based on the statistical analysis (Figure 3), covers the power demand for >90% of the tug's operating time. For the rare instances requiring sustained power above 250 kW when the battery is depleted, the system would need to operate at a reduced power, but the operational data suggests this scenario is highly unlikely. Therefore, based on simulation results, the proposed system is expected to match or exceed the original vessel's performance for all practical operational scenarios, pending detailed integration study and validation. Regarding system integration, the additional weight (approximately 3–4 t) and volume of the battery and power electronics are considered manageable within the vessel's layout and can be accommodated without compromising stability, pending a detailed shipyard integration study.

4.3. Effectiveness and Evolution Potential of the EMS

The rule-based hierarchical strategy designed in this study demonstrated good performance in simulation but is essentially reactive control. Future enhancements can be made in the following directions.

(a) Predictive Energy Management (PEM): Integrate ship operation schedules, electronic charts, weather forecasts, etc., to predict power demand for future voyage segments, thereby optimizing the SOC trajectory and engine start/stop plans in advance. For example, starting the engine earlier to charge the SOC to a higher level before intensive operations, attempting to use battery power as much as possible before berthing to lower the SOC to a level suitable for receiving shore power.

(b) Adaptive Strategy Based on Machine Learning/Reinforcement Learning (RL): Collect large amounts of actual ship operation data to train an intelligent agent to learn optimal power allocation strategies. RL strategies can better handle complex, nonlinear system dynamics and uncertain environmental disturbances, potentially achieving better long-term average performance than rule-based and MPC strategies.

(c) Multi-Objective Real-Time Optimization: Explicitly incorporate battery life degradation models, emission costs, etc., into the control strategy to achieve online multi-objective trade-off optimization among economy, environmental performance, and equipment lifespan.

4.4. Practical Considerations: Methanol Fuel Supply and Bunkering

The economic analysis presented in Section 3.3.2 relies on assumptions regarding methanol availability and pricing. While methanol is a globally traded commodity, its widespread adoption as a marine fuel is still nascent [64]. The current bunkering infrastruc-

ture for methanol is limited compared to conventional fuels, posing a practical challenge for immediate, widespread implementation. However, significant developments are underway. Major ports are initiating projects to establish methanol bunkering capabilities, driven by the growing order book for methanol-fueled newbuilds [65]. The cost of green methanol is currently higher than its fossil-based counterpart, but its production cost is projected to decrease significantly with the scaling up of renewable energy and carbon capture technologies [66]. Therefore, while this study's analysis provides a robust baseline based on current favorable pricing for fossil methanol, the long-term viability and environmental superiority of the concept are contingent on the parallel development of a green methanol supply chain. This study's framework can be readily adapted to assess scenarios with different methanol prices and origins (fossil vs. renewable) as the market evolves. Therefore, the practical implementation of the proposed system is contingent upon the parallel development of methanol bunkering infrastructure at the port of operation, and this should be considered as an external constraint in any deployment plan.

4.5. Challenges of Methanol Fuel Application and System Integration Considerations

Although methanol has obvious advantages, engineering applications must properly address the following challenges.

(a) Material Compatibility and Safety: Targeted material selection (e.g., stainless steel, Teflon coating) is required for fuel delivery pipelines, storage tanks, pumps, and valves. A complete safety system, including methanol leak detection, forced ventilation, water mist firefighting, and personnel protection, must be installed.
(b) Cold Start and Combustion Stability: Methanol's high latent heat of vaporization may cause cold start difficulties. Technical measures such as intake air preheating, a higher compression ratio, or spark plug-assisted ignition (for retrofitted dual-fuel engines) are needed.
(c) System Integration Complexity: Heat dissipation, electromagnetic compatibility (EMC), vibration, and protection of high-power electronic equipment within the limited space of a ship are significant challenges. Careful design of liquid cooling systems, electromagnetic shielding, and filtering solutions, along with rigorous land-based integration testing, is required.
(d) Redundancy and Reliability Design: For vessels such as harbor tugs with extremely high safety requirements, redundancy configurations (e.g., dual-winding motors, parallel inverters) should be considered for propulsion inverters, control systems, etc., to ensure basic maneuvering capability is maintained in case of a single-point failure.

4.6. Research Limitations and Future Work Outlook

The main limitations of this research include the following:

(a) The simulation is based on a specific duty cycle and idealized component models; future validation requires more extensive actual ship operational data and Hardware-in-the-Loop (HIL) testing.
(b) The economic analysis is based on current market prices and specific assumptions; long-term trends (e.g., green methanol price reduction, carbon tax policies) will influence the conclusions.
(c) The impact of low-temperature environments on battery performance, engine starting, and corresponding mitigation measures was not discussed in detail.

Future work will focus on the following:

(a) Developing and implementing PEM algorithms and validating their advantages first through Model-in-the-Loop (MIL) and then on HIL simulation platforms. HIL testing, incorporating real BMS and motor controller hardware, will provide a more

realistic assessment of the control system's dynamic performance and robustness before proceeding to a full-scale prototype or ship retrofit.

(b) Conducting an actual ship retrofit demonstration project on a harbor tug. This will involve collecting full life-cycle operational data to validate the simulated economic and environmental benefits, and to explore practical challenges of system integration, safety, and reliability in a real-world marine environment.

(c) Researching the full-chain application of green methanol (e-methanol). This includes assessing its full life-cycle carbon-neutral potential, analyzing the future supply chain and bunkering infrastructure for renewable methanol in ports, and conducting comparative techno-economic studies with other future fuel pathways such as hydrogen and ammonia.

(d) Investigating the impact of battery aging on long-term system performance. This involves integrating a battery SOH model into the simulation framework. This will allow us to study how increasing internal resistance and capacity fade affect the system's power delivery capability and overall energy efficiency over the battery's lifetime, enabling the development of aging-aware energy management strategies that optimize for both fuel economy and battery longevity.

5. Conclusions

This study systematically proposed and validated a comprehensive design methodology for a methanol range-extended series hybrid powertrain system, specifically targeting the operational challenges of harbor tug operations. The key conclusions, which directly validate the scientific contributions outlined in the introduction, are as follows.

(a) Validation of Data-Driven Design Methodology: The quantitative analysis of the harbor tug's operational profile (peak 633.2 kW, average 189.9 kW, 86.8% of time below 300 kW) provided a precise, data-driven foundation for system design. The high correlation ($R^2 = 0.9968$) between the simulated power demand and parent ship data confirms the accuracy of this study's load profiling model.

(b) Proof of the "Battery-Dominant, Engine-as-APU" Paradigm: The simulation results provide strong evidence for this paradigm. The 200 kW·h/600 kW battery pack successfully buffered all transient load spikes, while the 250 kW methanol APU, when activated, operated at a steady > 42% efficiency for 35% of the cycle, completely decoupled from load fluctuations. This validates the core principle of decoupling energy and power for efficiency gain.

(c) Effectiveness of the Hierarchical EMS: The proposed rule-based EMS effectively managed mode transitions (single engine start), maintained SOC within a safe range (28–80%), and enabled 62% regenerative braking energy recovery. This demonstrates that the designed control strategy can translate the hardware's theoretical potential into tangible operational benefits.

(d) Demonstration of Multi-Faceted Benefits: The integrated assessment framework confirmed the system's overall superiority. It achieved a 50.8% fuel saving rate, a sub-3-month investment PBP (with robust sensitivity), and dramatic emission reductions (94.8% for CO_2, 95% for NO_x). These results collectively demonstrate the technical, economic, and environmental feasibility of the proposed solution.

In summary, the proposed methanol range-extended series hybrid powertrain system is technologically advanced, economically highly competitive under the assumed conditions, and environmentally friendly—particularly when using green methanol. It not only provides an immediately viable optimal pathway for the green upgrading of existing port fleets but also sets a new benchmark for powertrain system selection in newbuild vessels. With the maturation of the green methanol industry and advancements in battery

technology, the application prospects of this scheme will be even broader, and it is poised to make substantial contributions to the sustainable development of global ports and the deep decarbonization of the shipping industry.

Author Contributions: Conceptualization, W.L.; methodology, Z.L.; software, Z.L.; validation, H.T.; formal analysis, Z.L.; investigation, Z.L.; resources, Z.L.; data curation, W.L.; writing—original draft preparation, Z.L.; writing—review and editing, W.L.; visualization, Z.L.; supervision, W.L.; project administration, H.T.; funding acquisition, H.T. All authors have read and agreed to the published version of the manuscript.

Funding: This research received no external funding.

Data Availability Statement: The data presented in this study are available on request from the corresponding author.

Acknowledgments: The authors acknowledge the technical support and experimental materials provided by the Institute of Internal Combustion Engine Research, School of Energy and Power Engineering, Dalian University of Technology.

Conflicts of Interest: The authors declare no conflicts of interest.

Abbreviations

AIS	Automatic Identification System
APU	Auxiliary Power Unit
BMS	Battery Management System
BSFC	Brake Specific Fuel Consumption
CAPEX	Capital Expenditure
CO2	Carbon Dioxide
DAB	Dual Active Bridge
DC	Direct Current
DOD	Depth of Discharge
ECAs	Emission Control Areas
EMC	Electromagnetic Compatibility
EMS	Energy Management Strategy
HESS	Hybrid Energy Storage System
HEMS	Hierarchical Energy Management Strategy
HEV	Hybrid Electric Vehicle
HIL	Hardware-in-the-Loop
IMO	International Maritime Organization
IRR	Internal Rate of Return
LFP	Lithium Iron Phosphate
LFPBP	Lithium Iron Phosphate Battery Pack
MAU	Modified Au-type
MIL	Model-in-the-Loop
MPC	Model Predictive Control
NOx	Nitrogen Oxides
NPC	Neutral Point Clamped
NPV	Net Present Value
OPEX	Operational Expenditure
PBP	Payback Period
PHEBs	Plug-in Hybrid Electric Buses
PHEVs	Plug-in Hybrid Electric Vehicles
PEM	Predictive Energy Management
PM	Particulate Matter
PMSM	Permanent Magnet Synchronous Motor

PMSG	Permanent Magnet Synchronous Generator
RL	Reinforcement Learning
SCR	Selective Catalytic Reduction
SOH	State of Health
SOC	State of Charge
SOx	Sulfur Oxides
VDC	Volts Direct Current
VDR	Voyage Data Recorder
WACC	Weighted Average Cost of Capital

References

1. Sepehri, A.; Kirichek, A.; Heuvel, M.; Koningsveld, M. Smart, sustainable, and circular port maintenance: A comprehensive framework and multi-stakeholder approach. *J. Environ. Manag.* **2024**, *370*, 122625. [CrossRef]
2. Wang, H.; Zhou, P.; Liang, Y.; Jeong, B.; Mesbahi, A. Optimization of tugboat propulsion system configurations: A holistic life cycle assessment case study. *J. Clean. Prod.* **2020**, *259*, 120903. [CrossRef]
3. Tan, S.; Xie, P.; Norman, R. Advancements in Power Management Systems for Hybrid Electric Vessels. *J. Mar. Sci. Eng.* **2025**, *13*, 794. [CrossRef]
4. Mushtaq, R.; Iqbal, M.; Khaliq, A.; Iqbal, J. Optimal design of a hybrid ship energy management system under various sea conditions using Model Predictive Control. *PLoS ONE* **2025**, *20*, e0326969. [CrossRef]
5. Murcia González, J.C. Analysis and measurement of SO_x, CO_2, PM and NO_x emissions in port auxiliary vessels. *Environ. Monit. Assess.* **2021**, *193*, 374. [CrossRef]
6. Kondratenko, A.; Zhang, M.; Tavakoli, S.; Altarriba, E.; Hirdaris, S. Existing technologies and scientific advancements to decarbonize shipping by retrofitting. *Renew. Sustain. Energy Rev.* **2025**, *212*, 115430. [CrossRef]
7. Zhou, Z.; Tao, J. Hydrogen-powered vessels in green maritime decarbonization: Policy drivers, technological frontiers and challenges. *Front. Mar. Sci.* **2025**, *12*, 1601617. [CrossRef]
8. Zannis, T.; Katsanis, J.; Christopoulos, G.; Yfantis, E.; Papagiannakis, R.; Pariotis, E.; Rakopoulos, D.; Rakopoulos, C.; Vallis, A. Marine exhaust gas treatment systems for compliance with the IMO 2020 global sulfur cap and tier III NO_x limits: A review. *Energies* **2022**, *15*, 3638. [CrossRef]
9. Li, Z.; Long, W.; Lu, W.; Tian, H. Research on energy management strategy for marine methanol–electric hybrid propulsion system based on DP-ANFIS algorithm. *Energies* **2025**, *18*, 4879. [CrossRef]
10. Ammar, N.; Seddiek, I. Hybrid/dual fuel propulsion systems towards decarbonization: Case study container ship. *Ocean Eng.* **2023**, *281*, 114962. [CrossRef]
11. Tran, M.K.; Bhatti, A.; Vrolyk, R.; Wong, D.; Panchal, S.; Fowler, M.; Fraser, R. A review of range extenders in battery electric vehicles: Current progress and future perspectives. *World Electr. Veh. J.* **2021**, *12*, 54. [CrossRef]
12. Miretti, F.; Nicolotti, A.; Misul, D.; Ferrari, A. Emission-Optimal Control and Retrofit Potential of a Series Hybrid Powertrain for Urban Waterbuses. *Energies* **2025**, *18*, 4652. [CrossRef]
13. Sahoo, S.; Zhao, X.; Kyprianidis, K. A review of concepts, benefits, and challenges for future electrical propulsion-based aircraft. *Aerospace* **2020**, *7*, 44. [CrossRef]
14. Kim, Y.; Kim, J.; Jung, J.; Kim, S.; Choi, J.; Lee, H. Comprehensive design of dc shipboard power systems for pure electric propulsion ship based on battery energy storage system. *Energies* **2021**, *14*, 5264. [CrossRef]
15. Zhuang, W.; Li, S.; Zhang, X.; Kum, D.; Song, Z.; Yin, G. A survey of powertrain configuration studies on hybrid electric vehicles. *Appl. Energy* **2020**, *262*, 114553. [CrossRef]
16. Tran, D.; Vafaeipour, M.; Baghdadi, M.; Barrero, R.; Mierlo, J.; Hegazy, O. Thorough state-of-the-art analysis of electric and hybrid vehicle powertrains: Topologies and integrated energy management strategies. *Renew. Sustain. Energy Rev.* **2020**, *119*, 109596. [CrossRef]
17. Yuan, Y.; Wang, J.; Yan, X.; Shen, B.; Long, T. A review of multi-energy hybrid power system for ships. *Renew. Sustain. Energy Rev.* **2020**, *132*, 110081. [CrossRef]
18. Derollepot, R.; Vinot, E. Sizing of a combined series-parallel hybrid architecture for river ship application using genetic algorithm and optimal energy management. *Math. Comput. Simul.* **2019**, *158*, 248–263. [CrossRef]
19. Milićević, S.; Blagojević, I.; Milojević, S.; Bukvić, M.; Stojanović, B. Numerical Analysis of Optimal Hybridization in Parallel Hybrid Electric Powertrains for Tracked Vehicles. *Energies* **2024**, *17*, 3531. [CrossRef]
20. Nunes, L. Renewable Methanol as an Agent for the Decarbonization of Maritime Logistic Systems: A Review. *Future Transp.* **2025**, *5*, 54. [CrossRef]

21. Wu, P.; Lin, C. Feasibility and Cost-Benefit Analysis of Methanol as a Sustainable Alternative Fuel for Ships. *J. Mar. Sci. Eng.* **2025**, *13*, 973. [CrossRef]
22. Du, Y.; Shen, X.; Kammen, D.; Ding, X. Cost-competitive offshore wind-powered green methanol production for maritime transport decarbonization. *Nat. Commun.* **2025**, *16*, 5453. [CrossRef]
23. Al-Breiki, M.; Bicer, Y. Technical assessment of liquefied natural gas, ammonia and methanol for overseas energy transport based on energy and exergy analyses. *Int. J. Hydrogen Energy* **2020**, *45*, 34927–34937. [CrossRef]
24. Kanchiralla, F.; Brynolf, S.; Mjelde, A. Role of biofuels, electro-fuels, and blue fuels for shipping: Environmental and economic life cycle considerations. *Energy Environ. Sci.* **2024**, *17*, 6393–6418. [CrossRef]
25. Al Baity, O.; Ahmed, Y.; ElGohary, M.; Abdelnaby, M. Hybrid marine power systems: Techno-economic and environmental optimisation of alternative fuel pathways. *Brodogradnja* **2026**, *77*, 77304. [CrossRef]
26. Meddour, A.; Rizoug, N.; Leserf, P.; Vagg, C.; Burke, R.; Larouci, C. Optimization approaches for cost and lifetime improvements of lithium-Ion batteries in electric vehicle powertrains. *Energies* **2023**, *16*, 6535. [CrossRef]
27. Yuhimenko, V.; Baimel, D.; Sitbon, M.; Averbukh, M.; Lineykin, S.; Kuperman, A. Hybrid internal combustion engine based auxiliary power unit. *Micromachines* **2020**, *11*, 438. [CrossRef] [PubMed]
28. Yin, C.; Zeng, X.; Yin, Z. An improved data-driven predictive optimal control approach for designing hybrid electric vehicle energy management strategies. *Appl. Energy* **2024**, *375*, 123984. [CrossRef]
29. Wang, L.; Zhou, J.; Zhao, J. Optimization Research on Energy Management Strategies and Powertrain Parameters for Plug-In Hybrid Electric Buses. *World Electr. Veh. J.* **2024**, *15*, 510. [CrossRef]
30. Bai, Y.; Li, J.; He, H.; Santos, R.; Yang, Q. Optimal design of a hybrid energy storage system in a plug-in hybrid electric vehicle for battery lifetime improvement. *IEEE Access* **2020**, *8*, 142148–142158. [CrossRef]
31. Zhu, J.; Chen, L.; Wang, X.; Yu, L. Bi-level optimal sizing and energy management of hybrid electric propulsion systems. *Appl. Energy* **2020**, *260*, 114134. [CrossRef]
32. Hong, S.; Kim, D.; Kim, S. A back–forward approach-based efficiency performance analysis model for hybrid electric propulsion ships using the Holtrop–Mennen method. *J. Mar. Sci. Eng.* **2023**, *12*, 9. [CrossRef]
33. Ku, H.; Park, C.; Kim, J. Full simulation modeling of All-electric ship with medium voltage DC power system. *Energies* **2022**, *15*, 4184. [CrossRef]
34. Chen, H.; Zhang, Z.; Guan, C.; Gao, H. Optimization of sizing and frequency control in battery/supercapacitor hybrid energy storage system for fuel cell ship. *Energy* **2020**, *197*, 117285. [CrossRef]
35. Kolodziejski, M.; Michalska-Pozoga, I. Battery energy storage systems in ships' hybrid/electric propulsion systems. *Energies* **2023**, *16*, 1122. [CrossRef]
36. Akbarzadeh, M.; De Smet, J.; Stuyts, J. Battery Hybrid Energy Storage Systems for Full-Electric Marine Applications. *Processes* **2022**, *10*, 2418. [CrossRef]
37. Liu, H.; Lei, Y.; Fu, Y.; Li, X. Parameter matching and optimization for power system of range-extended electric vehicle based on requirements. *Proc. Inst. Mech. Eng. Part D-J. Automob. Eng.* **2020**, *234*, 3316–3328. [CrossRef]
38. Sun, Y.; Fang, Y.; Zhang, Q.; Liu, Q. Optimal design of marine motors for joint efficiency and economic optimization. *Energies* **2023**, *16*, 4588. [CrossRef]
39. Karimi-Ghartemani, M.; Khajehoddin, S.; Jain, P.; Bakhshai, A. A systematic approach to DC-bus control design in single-phase grid-connected renewable converters. *IEEE Trans. Power Electron.* **2012**, *28*, 3158–3166. [CrossRef]
40. Liu, H.; Fan, A.; Li, Y.; Bucknall, R.; Vladimir, N. Multi-objective hierarchical energy management strategy for fuel cell/battery hybrid power ships. *Appl. Energy* **2025**, *379*, 124981. [CrossRef]
41. Torreglosa, J.; González-Rivera, E.; García-Triviño, P.; Vera, D. Performance analysis of a hybrid electric ship by real-time verification. *Energies* **2022**, *15*, 2116. [CrossRef]
42. Kirca, M.; Calindi, S.; Whiffin, P.; Turner, M.; Parkes, D.; McGordon, A. A novel Multi-Input Multi-Output energy model for future port operations. *Int. J. Sustain. Transp.* **2025**, 1–17. [CrossRef]
43. Banaei, M.; Ghanami, F.; Rafiei, M.; Boudjadar, J.; Khooban, M.-H. Energy Management of Hybrid Diesel/Battery Ships in Multidisciplinary Emission Policy Areas. *Energies* **2020**, *13*, 4179. [CrossRef]
44. Maione, F.; Lino, P.; Maione, G.; Giannino, G. A Machine Learning Framework for Condition-Based Maintenance of Marine Diesel Engines: A Case Study. *Algorithms* **2024**, *17*, 411. [CrossRef]
45. Damian, S.; Wong, L.; Shareef, H.; Chan, C.; Moh, T.; Tiong, M. Optimal operation of diesel generator and battery energy storage system for total fuel cost minimization in hybrid power system. *J. Power Sources* **2025**, *628*, 235859. [CrossRef]
46. Ling-Chin, J.; Roskilly, A. Investigating the implications of a new-build hybrid power system for Roll-on/Roll-off cargo ships from a sustainability perspective–A life cycle assessment case study. *Appl. Energy* **2016**, *181*, 416–434. [CrossRef]
47. Li, C.; Wang, Z.; Liu, H.; Guo, F.; Xiu, X.; Qin, J.; Wei, L. 4E analysis of a novel proton exchange membrane fuel cell/engine based cogeneration system with methanol fuel for ship application. *Energy* **2023**, *282*, 128741. [CrossRef]

48. Lehmusto, M.; Santasalo-Aarnio, A. Mathematical framework for total cost of ownership analysis of marine electrical energy storage inspired by circular economy. *J. Power Sources* **2022**, *528*, 231164. [CrossRef]
49. Deepak, K.; Frikha, M.A.; Benômar, Y.; El Baghdadi, M.; Hegazy, O. In-Wheel Motor Drive Systems for Electric Vehicles: State of the Art, Challenges, and Future Trends. *Energies* **2023**, *16*, 3121. [CrossRef]
50. Li, P.; Jovcic, D.; Hodge, E.; Fitzgerald, J. Analysis of bidirectional 15 MW current source DC/DC converter for series-connected superconducting-based 1 GW/100 kV offshore wind farm. *Electr. Power Syst. Res.* **2022**, *202*, 107618. [CrossRef]
51. Zheng, Q.; Sun, L.; Chang, S.; Xing, H. Techno-Economic Analysis of Multi-Purpose Heavy-Lift Vessels Using Methanol as Fuel. *J. Mar. Sci. Eng.* **2025**, *13*, 1234. [CrossRef]
52. Mylonopoulos, F.; Coraddu, A.; Polinder, H. A holistic framework for optimal ship energy system design, including operational requirements, lifetime cost, and vessel stability. *Energy Convers. Manag. X* **2026**, *30*, 101685. [CrossRef]
53. Nie, A.; Wan, Z.; Shi, Z.; Wang, Z. Cost-benefit analysis of ballast water treatment for three major port clusters in China: Evaluation of different scenario strategies. *Front. Mar. Sci.* **2023**, *10*, 1174550. [CrossRef]
54. Nivolianiti, E.; Karnavas, Y.; Chatziaslanoglou, G. Techno-economic and life cycle cost analysis for hybrid short-sea passenger vessels based on optimization of different energy storage configurations and management. *Energy Convers. Manag.* **2025**, *343*, 120148. [CrossRef]
55. Mylonopoulos, F.; Durgaprasad, S.; Coraddu, A.; Polinder, H. Lifetime design, operation, and cost analysis for the energy system of a retrofitted cargo vessel with fuel cells and batteries. *Int. J. Hydrogen Energy* **2024**, *91*, 1262–1273. [CrossRef]
56. Letafat, A.; Rafiei, M.; Sheikh, M.; Afshari-Igder, M.; Banaei, M.; Boudjadar, J.; Khooban, M. Simultaneous energy management and optimal components sizing of a zero-emission ferry boat. *J. Energy Storage* **2020**, *28*, 101215. [CrossRef]
57. Truong, H.; Do, T.; Dang, T. Enhancing Efficiency in Hybrid Marine Vessels through a Multi-Layer Optimization Energy Management System. *J. Mar. Sci. Eng.* **2024**, *12*, 1295. [CrossRef]
58. Talluri, L.; Nalianda, D.; Kyprianidis, K.; Nikolaidis, T.; Pilidis, P. Techno economic and environmental assessment of wind assisted marine propulsion systems. *Ocean Eng.* **2016**, *121*, 301–311. [CrossRef]
59. Bahloul, M.; Khadem, S. An analytical approach for techno-economic evaluation of hybrid energy storage system for grid services. *J. Energy Storage* **2020**, *31*, 101662. [CrossRef]
60. Merkel, A.; Nyberg, E.; Ek, K.; Sjöstrand, H. Economics of shore power under different access pricing. *Res. Transp. Econ.* **2023**, *101*, 101330. [CrossRef]
61. Bajolle, H.; Lagadic, M.; Louvet, N. The future of lithium-ion batteries: Exploring expert conceptions, market trends, and price scenarios. *Energy Res. Soc. Sci.* **2022**, *93*, 102850. [CrossRef]
62. Gao, Q.; Bechlenberg, A.; Jayawardhana, B.; Ertugrul, N.; Vakis, A.; Ding, B. Techno-economic assessment of offshore wind and hybrid wind–wave farms with energy storage systems. *Renew. Sustain. Energy Rev.* **2024**, *192*, 114263. [CrossRef]
63. Karaçay, Ö.; Özsoysal, O. Techno-economic investigation of alternative propulsion systems for tugboats. *Energy Convers. Manag. X* **2021**, *12*, 100140. [CrossRef]
64. Parris, D.; Spinthiropoulos, K.; Ragazou, K.; Giovou, A.; Tsanaktsidis, C. Methanol, a Plugin Marine Fuel for Green House Gas Reduction—A Review. *Energies* **2024**, *17*, 605. [CrossRef]
65. Svanberg, M.; Ellis, J.; Lundgren, J.; Landälv, I. Renewable methanol as a fuel for the shipping industry. *Renew. Sustain. Energy Rev.* **2018**, *94*, 1217–1228. [CrossRef]
66. Osman, A.; Nasr, M.; Lichtfouse, E.; Farghali, M.; Rooney, D. Hydrogen, ammonia and methanol for marine transportation. *Environ. Chem. Let.* **2024**, *22*, 2151–2158. [CrossRef]

Disclaimer/Publisher's Note: The statements, opinions and data contained in all publications are solely those of the individual author(s) and contributor(s) and not of MDPI and/or the editor(s). MDPI and/or the editor(s) disclaim responsibility for any injury to people or property resulting from any ideas, methods, instructions or products referred to in the content.